RSC Advances

REVIEW

View Article Online
View Journal | View Issue

Cite this: *RSC Adv.*, 2023, **13**, 3976

A review: studying the effect of graphene nanoparticles on mechanical, physical and thermal properties of polylactic acid polymer

Kianoush Hatami Dehnou, *[a] Ghazal Saki Norouzi*[b] and Marzieh Majidipour[c]

Polylactic acid (PLA) is a linear aliphatic polyester thermoplastic made from renewable sources such as sugar beet and cornstarch. Methods of preparation of polylactic acid are biological and chemical. The advantages of polylactic acid are biocompatibility, easily processing, low energy loss, transparency, high strength, resistance to water and fat penetration and low consumption of carbon dioxide during production. However, polylactic acid has disadvantages such as hydrophobicity, fragility at room temperature, low thermal resistance, slow degradation rate, permeability to gases, lack of active groups and chemical neutrality. To overcome the limitations of PLA, such as low thermal stability and inability to absorb gases, nanoparticles such as graphene are added to improve its properties. Extensive research has been done on the introduction of graphene nanoparticles in PLA, and all of these studies have been studied. In this study, we intend to study a comprehensive study of the effect of graphene nanoparticles on the mechanical, thermal, structural and rheological properties of PLA/Gr nanocomposites and also the effect of UV rays on the mechanical properties of PLA/Gr nanocomposites.

Received 4th November 2022
Accepted 11th January 2023

DOI: 10.1039/d2ra07011a

rsc.li/rsc-advances

1. Introduction

Polylactic acid (PLA) is a linear aliphatic polyester thermoplastic made from renewable sources such as sugar beet and cornstarch.[1] Methods of preparing polylactic acid are biological and chemical.[2] The advantages of polylactic acid are biocompatibility,[3], low energy loss, transparency, high strength, resistance to water and fat penetration and low consumption of carbon dioxide[1] during production. However, polylactic acid has disadvantages, including hydrophobicity, brittleness at room temperature, low thermal resistance, slow degradation rate, permeability to gases, lack of active groups, and chemical neutrality.[4–10]

Applications of PLA include medical use for sutures and surgical implants.[10–15] Joints of surgical implants, such as pins and tubes, are also made of PLA, which breaks down in the human body within six months to two years.[15–18] It is also used in food packaging[18–20] and in the manufacture of disposable

[a]*Department of Materials Science and Engineering, School of Engineering, Shiraz University, Shiraz, Iran. E-mail: k.hatamidehnou714@gmail.com; k.hatamidehno@shirazu.ac.ir*

[b]*Chemical Engineering Department, Faculty of Engineering, Razi University, Iran. E-mail: gsnorouzi@gmail.com*

[c]*Chemical Engineering Department, Yasouj University, Yasouj 75914-35, Iran*

Kianoush Hatami Dehnou, born in 1994 in Yasouj city, Iran, graduated with a master's degree in materials engineering from Shiraz University, interested in polymers and working on the mechanical, thermal and rheological properties of polymers, especially polylactic acid and silicone rubber. Currently, he is doing various research projects with different universities in Iran and around the world.

Ghazal Saki Norouzi received her master's degree in chemical engineering at Razi University in Iran. She has worked on many projects in the areas of chemical and petroleum engineering. She has engaged in research in the field of polymers; processing and modifying the properties.

appliances,[21–24] home appliances and sanitary ware.[25–30] For this reason, PLA is known as a safe and secure plastic. The challenges of using polylactic acid in competition with industrial polymers are brittleness, high permeability to gases and water vapor, low glass transition temperatures, and poor thermal stability.[1]

To overcome these limitations, nanoparticles are added to PLA to improve its properties[30–35] one of these nanoparticles is graphene, which was discovered in 2004 and has unique properties.[36] Improves mechanical properties such as tensile strength and acts as an impermeable agent for oxygen transfer even at high temperatures.[37] Thus, the addition of graphene as a reinforcement agent improves the thermal, physical and mechanical properties of the polymer matrix.[38] Graphene has a hexagonal ring structure made of hexagonal carbon layers called graphite.[39,40] Graphene has outstanding properties such as high surface area, high yang modulus, fracture toughness and good thermal conductivity.[41]

Basically, polymer nanocomposites are polymer-based composites with at least one thermoplastic or thermosetting polymer backing phase and one nanometer-reinforcing phase.[42–47] Increasing nano-reinforcements improves ground phase properties compared to large-scale reinforcements.[48–51] These features include:

1. Thermal properties: increase of thermal resistance, decrease of thermal expansion coefficient, decrease of shrinkage.

2. Mechanical properties: increase in elastic modulus, strength, elongation and toughness, increase in abrasion resistance.

3. Chemical properties: improve chemical resistance.

4. Electrical properties: reduce electrical resistance.

5. Optical properties: reduce oxygen permeability and moisture.

2. Biodegradable plastics

Today, plastic has an important role and application in human daily life, such as packaging industries, general industries, pharmaceutical industries and medical industries. However, the massive consumption of these produced plastics leads to environmental pollution. Given this, the need to use materials that can be decomposed under environmental conditions is essential.[52] Today, bioplastics or biodegradable plastics have attracted a lot of attention.[53] Bioplastics can be extracted from plant materials such as starch[54] or synthetic biodegradable polymers such as polylactic acid,[55] polyvinyl alcohol[56–58] and poly(caprolactone). In addition, the degradation of bioplastics results in the production of carbon dioxide and water as the final product,[59–61] which is not harmful to the environment. Therefore, bioplastics are one of the newest materials that are classified as environmentally friendly products. However, bioplasts have disadvantages such as limited shelf life because they degrade faster and have less mechanical strength than conventional plastics.[62–68]

Biodegradable plastics based on energy resources can be divided into three broad categories:

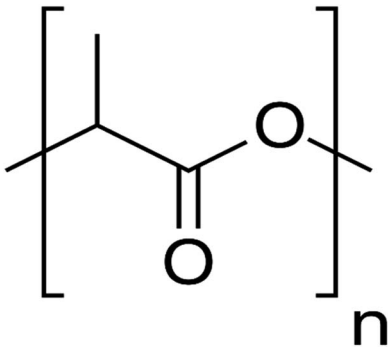

Fig. 1 PLA structure.[66]

1. Natural biopolymers such as carbohydrates, proteins and lipids derived from plants and animals;[68]

2. Renewable-based environmental polymers such as aliphatic polyesters, polycaprolactone polymers, polyvinyl alcohol and polylactic acid;[69]

3. Mixtures or composites of these biopolymers.[70]

3. Polylactic acid

Polylactic acid is a biodegradable Alligative polyester making from renewable sources such as starch, cotton, beets, corn, rye flour, wheat bran, barley starch, carrot waste, corn fiber and potatoes.[1] Lactic acid is made by fermenting corn or potato starch. The structure of PLA is shown in Fig. 1.

PLA is formed by polymerization. In the polymer synthesis general method for PLA, lactic acid compression polymerization and loop polymerization[67] are used. PLA biosynthesis is shown in Fig. 2.

PLA is currently the most important biodegradable polymer. PLA is a hydrophobic biopolymer that contains side methyl groups ($-CH_3$) with a glass transition temperature of 40 °C to 70 °C.[8] The tensile strength of PLA is usually in the range of 32 to 53 MPa.[68]

PLA can be processed by various methods such as injection molding, blow molding, sheet extrusion and processing. PLA films can also be made by various methods such as extrusion thermal forming, thermal compression and solvent casting.[70–76] PLA extrusion is the preferred method of high-performance production for applications such as packaging. Thermal compression method is also useful as a processing method due to its simplicity and ability to produce films without dissolving. Solvent casting is commonly used to make biopolymer films, which include the steps of solubilization, casting, and drying. Since PLA is soluble in a variety of solvents such as tetrahydrofuran, chloroform, benzene and dioxane, PLA film can be prepared by solution casting with any of these solvents.[76–81]

3.1. Benefits of PLA

PLA is an aliphatic polyester made from lactic acid. Biodegradable is biocompatible and inexpensive because it can be produced from renewable sources such as corn or sugarcane. PLA has several advantages over other biopolymers, such as:

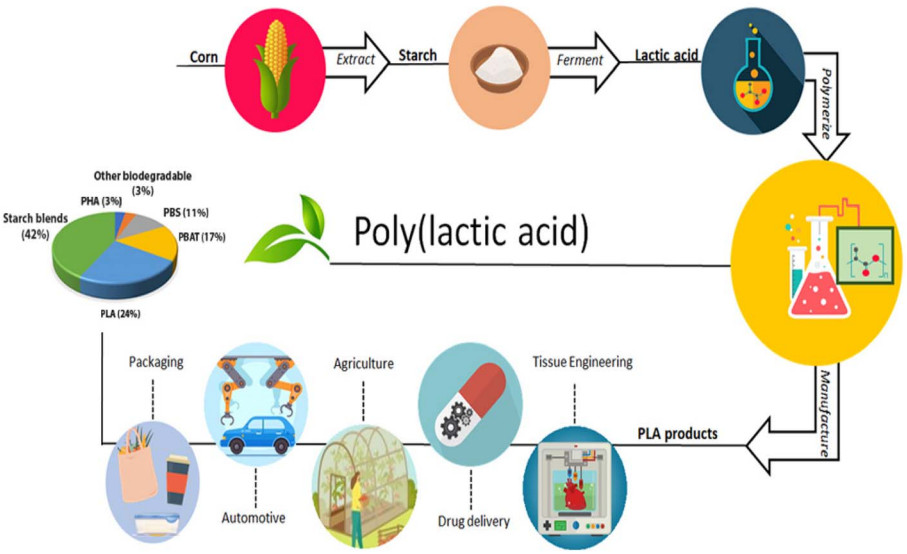

Fig. 2 PLA biosynthesis.[67]

1. Lactide monomer is obtained from lactic acid by fermentation from renewable sources.

2. Its production sources, such as corn fields, reduce the production of carbon dioxide.

3. Its production saves energy.

4. It can be recycled to alcohol or lactic acid by hydrolysis.

5. PLA can be used in the production of paper hybrid plastic packaging materials; 6- improves agricultural economy.[66]

3.2. Application of PLA

Due to its excellent mechanical properties, remarkable transparency and good processing ability compared to other biodegradable polymers, PLA is used in various fields such as textiles, paper coatings, food packaging and medicine.[82] PLA is widely used in biomedicine due to its environmental compatibility properties. PLA has been extensively studied for tissue engineering and drug delivery systems. For example, this polymer has several applications in tissue implant engineering and surgery, such as the production of flexible synthetic ligaments, screws, surgical plates and sutures, as well as in the production of nanoparticles and micro particles for drug delivery.[9,83–86]

3.3. Disadvantages of PLA

Some disadvantages such as vulnerability to heat, brittleness, slow crystal rate, poor mechanical properties and slow degradation rate limit the use of PLA.[87,88] Flame retardants and nano fillers are used.[89,90] Nano fillers are an interesting option, because by adding a small ratio of them, while maintaining the other basic properties of PLA, the final properties can be improved. Polymer matrix is available. The most commonly used nano fillers are: clay nanoparticles, carbon nanotubes and nanosilica.[86]

4. Graphene

4.1. Physical properties of graphene

For many years, graphene was considered a scientific material, where the monolayer structure of carbon atoms was merely a theoretical model for describing the properties of graphene-based materials such as graphite, fullerenes, and carbon nanotubes.[91–94]

Older theoretical predictions, in fact, the study of early two-dimensional crystals due to thermal fluctuations, assumed that graphene is unstable[95–99] because it prevents the formation of long-distance crystal order at finite temperatures. This idea was supported by various experimental studies on thin film layers. In those samples, the thickness of the apple was reduced by their instability. Now, in the early 21st century, graphene has emerged as a real example.[27,100–102]

Some of the important properties of graphene that have been reported so far include large surface to weight ratio (for example, 1 gram of graphene can cover several football fields), approximate elasticity of 1100 GPa,[103,104] fracture toughness of 125 GPa,[103,104] high thermal conductivity and high surface area (2630 $m^2 g^{-1}$)[105–111]

Since the fabrication of graphene, which consists of one or more graphite layers with SP^2 allotrope bonds of 2D carbon.[112–117] Due to its excellent properties such as thermal conductivity[117–125] and electrical conductivity,[126–131] high charge density,[132] mobility,[133] optical conductivity[134] and mechanical properties,[135] it has become a unique material. The main building blocks of carbon nanostructures are a graphite layer with SP^2 bonding covalently functionalized carbon atoms in a hexagonal honeycomb network (Fig. 3), which, when layers of a single graphite honeycomb network are entrained by a weak van der Waals bond force, they form a 3D graphite mass.[136]

When a graphite monolayer forms a sphere, it is known as a fullerene, and when it orbits its axis, it forms a one-

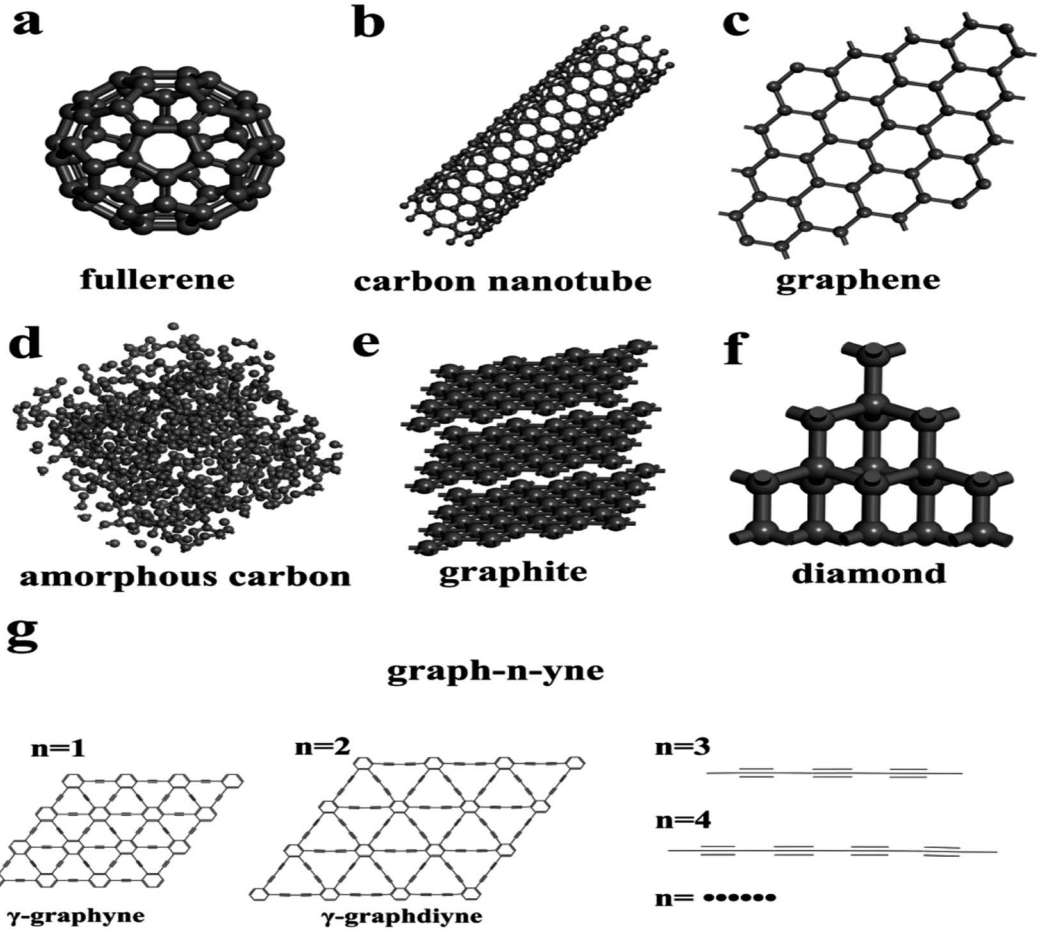

Fig. 3 Structures of different carbon materials. (a) Fullerene; (b) carbon nanotube; (c) graphene; (d) amorphous carbon; (e) graphite; (f) diamond; (g) GYs.[136]

dimensional cylindrical structure called a carbon tube, and when two sides form a two-dimensional structure, it is composed of one or more layers. Shows the formation, called graphite.

A graphite layer is known as a monoatomic graphene with a single atom, and two or three layers of graphite are known as a two-layer or three-layer graphene. Graphenes larger than 5 to 10 layers are commonly referred to as low-layer graphene, and graphenes with approximately 20 to 30 layers are called multilayer graphene, thick graphene, or thin nanocrystalline graphite.

4.2. Graphene synthesis

There are many reports on graphene synthesis, many of which are based on mechanical peeling of graphite,[137,138] reduction of graphene oxide[139,140] and, more recently, chemical vapor deposition.[141–143]

4.3. Mechanical peeling

Mechanical peeling is the first known method in the synthesis of graphene.[144] This is a top-down method in nanotechnology that produces a longitudinal or transverse pressure on the surface of a layered structure material using a simple adhesive tape with an AFM tip to cut a single layer or layer of material into a single layer. Graphite is formed when layers of monoatomic graphene are bonded together by van der Waals forces.[145]

4.4. Chemical peeling

Chemical peeling is the process by which alkali metals are added to the structure of graphene to separate the multilayer graphene dispersed in solution.[146,147] Alkali metals are materials that can easily form graphene intermediate structures with measurement ratios of different graphite elements in alkaline metals.[148]

4.5. Chemical synthesis of graphene from reduced graphene oxide

Chemical synthesis is a top-down indirect graphene synthesis method, and the first chemical method is graphene synthesis. This method involves the synthesis of graphite oxide by graphite oxidation, the dispersion of graphite flakes by ultrasonic agent and its reduction to graphene. Three common methods are available for GO synthesis. Brody method, Meyer method and Hummers' method. These three methods include graphite oxidation using strong acids and oxidants. The degree of oxidation can vary depending on the reaction conditions (*e.g.*,

temperature, pressure, and stoichiometric type). Hummer[149] proposed a method for making graphene by mixing graphite with sodium nitrate, sulfuric acid, and potassium permanganate, known as the Hummers' method.

4.6. Benefits of graphene

Graphene, the new allotropic carbon, due to its remarkable electronic,[150] thermal[151] and mechanical[104] properties, has been considered as an excellent mineral filler for the preparation of polymer-based nanocomposites[152,153] with very low loading materials.[88] Applications in nanocomposites, energy storage devices, various biomedical applications such as gene transfer, drug delivery, protein release, tissue engineering, imaging, anesthesia and packaging are some of the applications of graphene.[86] Graphene has recently been recognized as a potential nano filler for the production of polymer nanocomposites.[154,155] This material has many properties such as mechanical strength and thermal conductivity (5000 W m^{-3} K^{-1})[156] which is much higher than the certified standards for single wall CNTs. In addition to the very high level (2630 m^2 g^{-1}), these properties together with gas permeability indicate the future applications of graphene to improve the mechanical, thermal and gas barrier properties of polymeric materials.[157] Graphene oxide (GO) is similar to graphene, but has several oxygen-containing functional groups (such as hydroxyl epoxides and carbonyls). The presence of these polar groups reduces the thermal stability of nanomaterials, but may be to enhance interaction and compatibility with a particular polymer matrix.[86]

5. Polylactic acid and graphene nanocomposites

Only a small amount of graphene is required to reinforce PLA, these nanocomposites can be used in medical food preservatives and biomedical technologies.[86,158,159]

5.1. Methods of preparation of PLA-Gr nanocomposite

A composite is made up of two or more components.[160,161] Usually, if the polymer base phase and the other phase use nanomaterials, that material is called nanocomposite.[162,163] In the case of nanocomposites, mechanical and thermal properties are increased by adding a small percentage of nanometer amplifiers.[164–168] The uniform distribution of the amplifier phase creates a large interface between the nanometer amplifier phase and the matrix ground phase. There are two major challenges to producing a nanocomposite. In the first step, select the nanoparticles in such a way that it creates the necessary compatibility with the ground phase and also can create the expected properties. In the second step, a suitable method for the production of nanocomposites must be selected so that a suitable distribution of the amplifier takes place in the ground phase.[169,170] Preparation of nanocomposites by three methods of *in situ* polymerization,[171] melt mixing[172,173] and solution,[174,175] for polymer nanocomposites has long been industrially developed and used.

5.1.1. *In situ* polymerization method. *In situ* polymerization method, the distribution of nanoparticles is considered. This method creates a very good interface between the reinforcing particles and the ground. Graphene-containing polymer nanocomposites with high electrical conductivity and low permeability are prepared by this method.[176,177] By surface modification,[178,179] the proper distribution of nanoparticles can be done uniformly to prevent clumping of the nanometer components of the nanoparticles and to provide a proper distribution of the amplifier phase.

5.1.2. Melt mixing method. This method involves mixing polymers and nanoparticles at a high glass transition temperature or polymer melting point. After mixing, the mixture is cooled to the transition temperature of glass and a nanocomposite structure is formed. In this method, due to the ground melt state, mixers such as single-screw, double-screw extruders and internal mixers are used. In the melt mixing method, the establishment of polymer chains will depend on the proper interaction between the nanoparticles and the polymer substrate. Melt mixing has limitations for the nanocomposite production process, the most important of which are the formation of defects and cavities in the field as well as the inability to distribute uniformly for particles with different morphologies.[172,173]

5.1.3. Solution method. The solution method is based on the fact that the polymer, solubility and nanoparticles can be properly distributed in the solvent. In this way, polymer nanocomposites can be produced in two ways. If the polymer substrate and the nano fibers are miscible, the resulting solution can be cast into a mold and the nanocomposite produced,[180,181] otherwise the nanocomposite mixture is dissolved in a solvent and finally the nanocomposites are obtained by evaporation of the solvent. The solution method mainly consists of two steps. In the first step, by mixing the polymer solution and nano particles distributed in a solvent, the polymer chains are distributed between the nanoparticles. In the second step, the solvent is obtained by evaporation or precipitation of the nanocomposite.

The solution method is suitable for non-polar polymers, or polymers with low polarity with nanoparticles.

So far, several graphene polymer nanocomposites prepared by solution method, melt method[182,183] or *in situ* polymerization[184,185] have been reported. Among these methods, the solution method is widely used and can be used to facilitate mixing and dispersion of graphene due to the low viscosity of the mixing system in solution. One of the key points in solution formulation is to use a suitable solvent to create a uniform composition of polymers and nanofillers.[186,187]

5.1.4. Preparation of PLA/Gr nanocomposite samples. Chen *et al.*[87] produced a PLA/Gr nanocomposite using a solution method. In this research, first graphene oxide was produced by using Hummers' method and then by annealing it at 1050°, graphene powder was obtained. The graphene was then dispersed in chloroform by ultrasonic method at a concentration of 0.2 mg ml^{-1} by ultrasonic for 2 hours and left in the same state for one month to determine whether the graphene

Table 1 Different PLA-Gr nanocomposite samples preparation method

Name	Year	Sample preparation method
Chen *et al.*[87]	2011	Dissolve graphene in chloroform by ultrasonic for 2 hours, keep for 1 month in the same state, add PLA and chloroform mixture to graphene-chloroform mixture, dry samples for 12 hours in a vacuum oven at 75 °C
Chartarrayawadee *et al.*[62]	2017	Dissolve 8.91 g of PLA resin in 45 ml THF at 50 °C, dry in an oven vacuum at 70 °C for 12 hours, dissolve 009 g of graphene oxide by sonication in 30 ml, THF for 30 minutes, mix graphene oxide solution with PLA solution, prepare PLA-GO composite films by a hot pressure process by pressing and heat the powder for 60 minutes at 180 °C
Valapa *et al.*[157]	2015	Dissolve 0.95 g of PLA in 30 ml, chloroform by continuous shaking for 2 hours, disperse graphene by weight ratios (0.1, 0.1 and 0.5) wt% in 20 ml, chloroform in sonication bath for 30 minutes, adding the two solutions together and placing the sonication bath for 15 and 30 minutes, drying the solution on Teflon plates for 24 hours
Chan *et al.*[191]	2015	Dry PLA at 105 °C for at least 4 hours before use, dissolve GO in acetone solvent and then chloroform for 20 minutes and sonicate and homogenize, dissolve PLA at 40 °C in chloroform, add suspension GO in chloroform to solution to achieve weight ratios (0.1, 0.2, 0.3, 0.4 and 0.5), drying in an oven at 35 °C

was lumpy. After one month, a mixture of PLA and chloroform was added to the graphene-chloroform mixture, and finally the obtained samples were dried in a vacuum oven at 75 °C for 12 hours and kept in a desiccator until use.

In a study by Chartarrayawadee *et al.*,[62] in the first stage, 8.91 g of PLA resin in 45 ml of tetrahydrofuran (THF) was shaken continuously at 50 °C until the PLA was completely dissolved in a vacuum oven at 70 °C was dried for 12 hours. 0.09 g of graphene oxide was dissolved by sonication in 30 ml, THF for 30 minutes at room temperature. Graphene oxide solution (GO) was mixed with PLA solution and a powder mixture was prepared. PLA-GO composite films were made by a hot pressing process that involves compressing and heating the powder for 60 minutes at 180 °C.

Valapa *et al.*[157] initially dissolved 0.95 g of PLA in 30 ml of chloroform by continuous shaking for 2 h. Graphene was dispersed in the sonication bath for 30 minutes at weight ratios (0.1, 0.3 and 0.5%) by weight in 20 ml of chloroform.

The two solutions were then added and placed in a sonication bath for 15 to 30 minutes. The resulting solution was then placed on Teflon plates for 24 hours to dry. The dried composite films were carefully separated and the resulting films were dried at 40 °C for 12 hours and stored in impermeable bags.

Zhan *et al.*[188] prepared nanocomposite films (PLA-ODAG) (alkylated graphene sheets) by a solution method using chloroform solvent. The ODAG was dispersed for 30 minutes at room temperature in 5 mg ml^{-1} chloroform in an ultrasonic bath. PLA was also dissolved in chloroform at room temperature. A quantity of ODAG-$CHCL_3$ was then added to the PLA solution under sonication. Pour the homogeneous solution into a clean glass plate to obtain PLA-ODAG films for one hour, and allow the solvent to dry completely in a vacuum at 48 °C for 48 hours. PLA-ODAG nanocomposite films with thickness (30 μm) were made with a weight percentage of 0.1–1.

Huang *et al.*[82] prepared nanocomposite films with values (0–0.25–0.5–1–2) weight percent. First, GONS (graphene oxide nanofibers) was added to 200 ml of *N–N* dimethylformamide (DMF) solvent and formed a stable and uniform suspension by ultrasonic at room temperature for 2 hours. 10 g of PLA granules were added to 200 ml of DMF. Homogeneous PLA-GONS solution was added to a large amount of water and the accumulated material was precipitated. After accumulation, they were separated by filtration and dried in an oven at 60 °C. The films were then prepared by compression molding and cooled to room temperature at 10 MPa for 5 minutes.

Kuang *et al.*,[189] PLA-GO (graphene oxide) nanocomposites were prepared using *N–N* dimethylformamide (DMF) solvent. PLA was completely dissolved in DMF at a concentration of 100 mg ml^{-1} with the help of an agitator and an ultrasonic bath at 80 °C for 4 hours. The desired amount of GO was also added to the DMF. After homogeneous mixing, the solvent was evaporated at 105 °C for 24 hours in a vacuum and the PLA-G0 nanocomposite film was dried at 80 °C in a vacuum oven. GO to PLA ratios are 0.2, 0.4, 0.6, 0.8 and 1 wt%.

Kim *et al.*[190] first dissolved the PLA resin in THF solvent magnetically to obtain a homogeneous solution. Then some GO suspension in water was added to the PLA solution. The PLA-GO solution was placed in a sonication bath for 15 minutes to precipitate a layer of graphite. The resulting solution was dispersed homogeneously on the glass layer using a micrometer. The films were then dried for 60 minutes at 60 °C in a vacuum oven. After the drying process, a thin sheet of PLA-GO film was carefully removed from the glass substrate.

Chan *et al.*[191] for the production of PLA nanocomposite film reinforced with graphene oxide. The PLA was first dried at 105 °C for at least 4 hours before use. GO is first dissolved in acetone solvent and then chloroform and sonicated and homogenized for 20 minutes. PLA was dissolved in chloroform at 40 °C until all granules were dissolved. Amounts of GO suspension in chloroform were added to the solution to obtain weight ratios (0.1, 0.2, 0.3, 0.5). The resulting suspensions are poured into a special container and dried in an oven at 35 °C.

Zhao *et al.*[192] developed the PLA/GO nanocomposite using the following steps. PLA was first dissolved in chloroform and

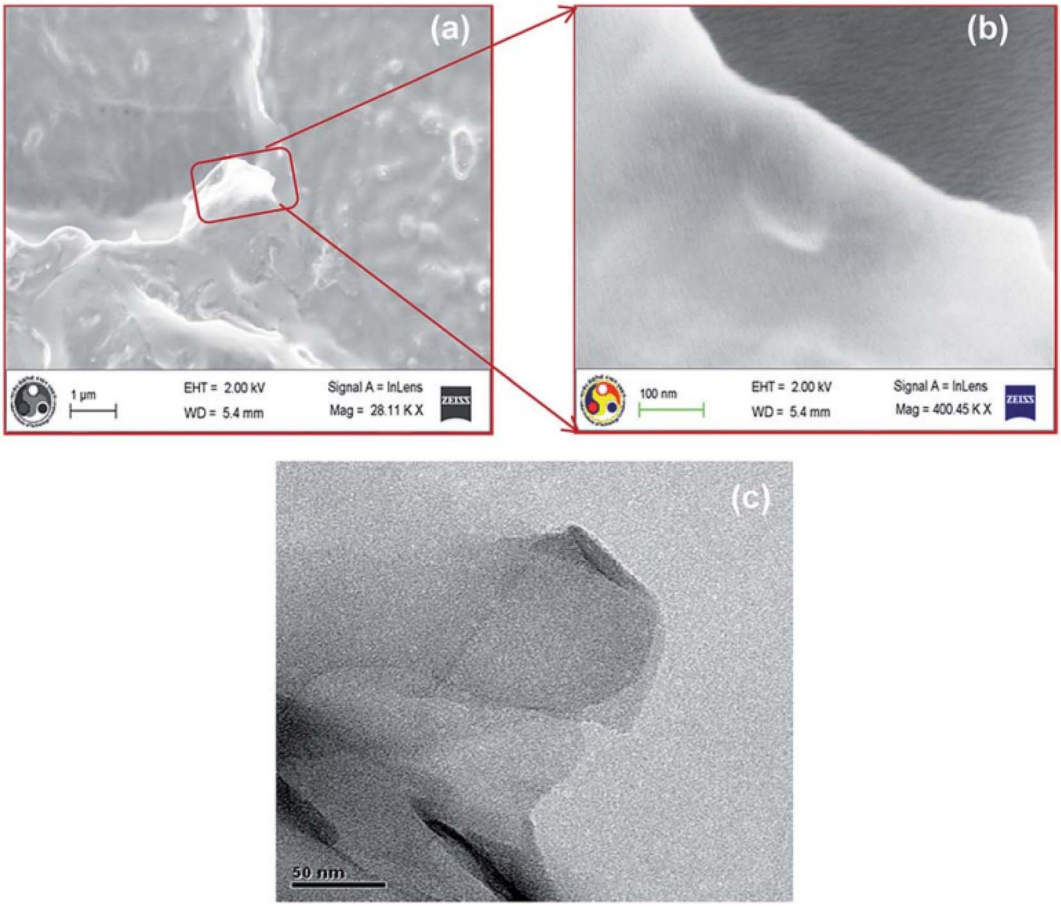

Fig. 4 FE-SEM images of (a) PLA-GR composite (low magnification) (b) PLA-GR composites (high magnification) and (c) TEM image of PLA-GR-0.1. ($T = 25$ °C).[157]

then rapidly poured into methanol and finally dried under vacuum before use. GO was produced in the laboratory from natural graphite according to the modified Hummers' method.

In the process of preparing a sample of PLA/GO composites, GO was dispersed in THF by ultrasonic for 90 minutes at room temperature. A certain amount of PLA was also dissolved in THF at a concentration of 100 mg ml^{-1}. The PLA solution with a volume of 20 ml and the GO solution with 10 ml of THF are mixed and mixed with a magnetic stirrer to form a homogeneous mixture. In Table 1, the sample preparation methods discussed in the articles are presented in the form of a table.

6. The effect of nanoparticles on the properties of PLA matrix

6.1. Morphology of samples

Using TEM and FE-SEM images in Fig. 4, Valapa *et al.*[157] found that graphene with a corrugated structure was homogeneously dispersed in the PLA matrix and no aggregation was observed in the nanocomposite.

Chartarrayawadee *et al.*[62] examined the surface topography and morphology of GO-, GO-GO-SA1: 3, SA1: 1, and GO-SA1: 5 using SEM at magnification of 1000× and 5000× (Fig. 5). At high magnification, they observed wrinkles on the GO surface. When stearic acid (SA) is added, GO appears to be encapsulated by stearic acid. PLA-GO, PLA, GO-SA1: 3, GO-SA1: 1 and GO-SA1: 5 failure levels were also observed. PLA-GO fracture surfaces PLA is quite rough and has many holes and brittle failure with some heterogeneous phases of GO in the PLA matrix. Samples containing stearic acid have softer levels and the refractive index is soft, indicating that GO is more compatible with PLA due to the presence of stearic acid.

Wu *et al.*[193] examined the surface topography and morphology of PLA/nGO@starch10, PLA/nGO@starch20, and PLA/nGO@starch30 using SEM (Fig. 6). At high magnification, they observed wrinkles on the GO surface. When stearic acid (SA) is added, GO appears to be encapsulated by stearic acid. PLA/nGO@starch10, PLA/nGO@starch20, PLA/nGO@starch30 failure levels were also observed. PLA-GO fracture surfaces PLA is quite rough and has many holes and brittle failure with some heterogeneous phases of GO in the PLA matrix. Samples containing stearic acid have softer levels and the refractive index is soft, indicating that GO is more compatible with PLA due to the presence of stearic acid.

Valapa *et al.*,[157] using morphological images in Fig. 7, observed that the dispersion of graphene sheets in the polymer

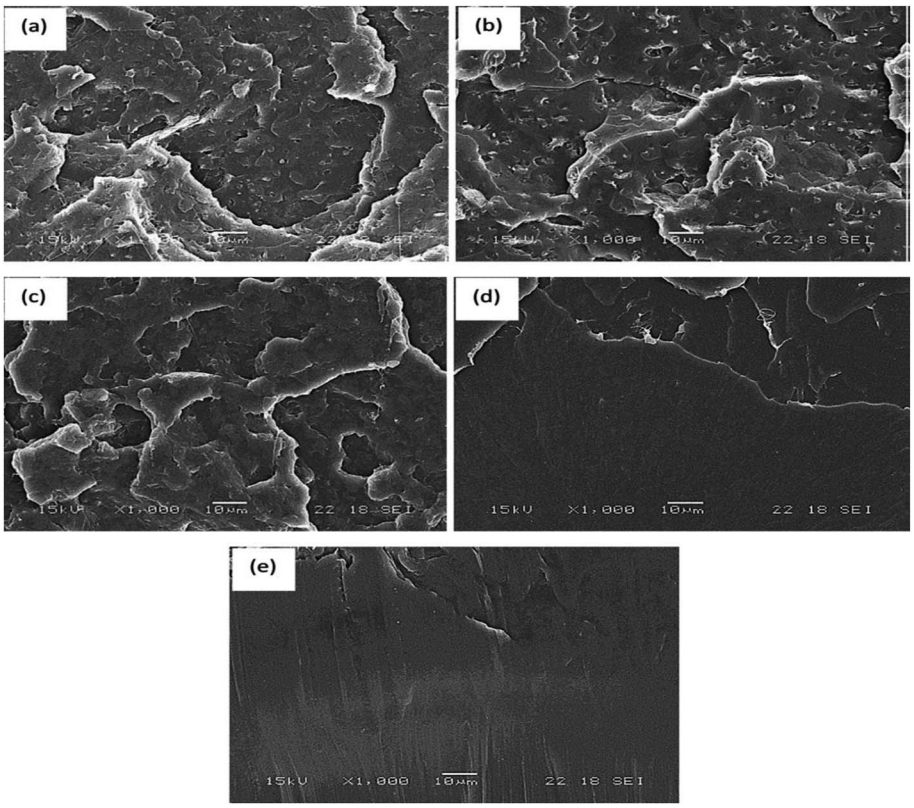

Fig. 5 Cross-sectional SEM images of composite films at 1000× magnification of (a) PLA, (b) PLA-GO, (c) PLA-GO-SA1:1, (d) PLA-GO-SA1:3, and (e) PLA-GO-SA1:5.(T = 25 °C) (this figure has been adapted from ref. 62 with permission from Wiley, copyright 2015).

matrix and the formation of bonds with each other increase the physical and mechanical properties of composite materials.

Using SEM images, Zhang *et al.*[188] found that pure PLA had smooth fracture surfaces with a number of cracks, indicating brittle fracture behavior at low temperatures. PLA-ODAG is relatively coarse and dense due to the interfacial stress of PLA and ODAG. The SEM image of the fracture surface of polylactic acid and related composites is shown in Fig. 8.

Using SEM images, Huang *et al.*[82] observed smooth refractive levels in pure PLA and very rough surfaces in PLA-GONS nanocomposites. They also found that GONS were held very tightly in the polymer matrix, a result that could be attributed to the excellent compatibility or strong adhesion between the GONS and the PLA matrix due to the hydrogen bond between the oxygen-containing groups on the GONS layer and the ester groups in the PLA molecular chain.

Kuang *et al.*[189] studied the microstructure of GO synthesis using TEM and AFM. The FTIR results clearly show that different types of oxygen-containing active groups on GO are presented.

Kim *et al.*[190] compared the structure of graphene oxide and low functionalized graphene oxide (LFGO) using TEM images and XRD analysis and found that the distribution of graphene in graphene oxide was better than LFGO and the resulting nanocomposite has a more interlayer structure than LFGO. Also, with increasing graphene, the number of accumulated layers increases.

6.2. Thermal behavior and crystallization of PLA nanocomposites

Using DSC analysis, Chen *et al.*[87] the addition of graphene to the PLA matrix had a slight change in melt temperature T_m and was slightly higher than pure PLA, indicating that graphene could reduce the mobility of polymer chains. Also, the cold crystallization temperature of the nanocomposite shifts to higher values compared to pure PLA.

Chen *et al.*[88] continue the previous work by studying the PLA/Gr microstructure under non-isothermal crystallization. In this study, the cooling rate in the DSC test was not the same and varied from 0.5 to 4 °C min^{-1}. Its diagram can be seen in reference number [47]. It is clear that as the cooling rate increases, the T_P and T_C temperatures decrease. He also attempted to model the asynchronous crystallization of PLA/Gr nanocomposites using Qzawa Avrami models, and the model developed by Olivier *et al.*,[66] which was only possible with the latter method. DSC thermograms of different PLA nanocomposites shows in Fig. 9.

Chartarrayawadee *et al.*,[62] from observations of DSC analysis (Fig. 10), found that the addition of GO did not affect T_g and T_m; Addition of stearic acid reduces T_m and T_g because it has a emollient effect and increases the compatibility of GO particles with the PLA matrix, which leads to a nucleation effect in the matrix. Nanoparticles in the matrix act as nucleating centers for crystallization, but only if the nanoparticles are well dispersed and have minimal interphase adhesion to the PLA

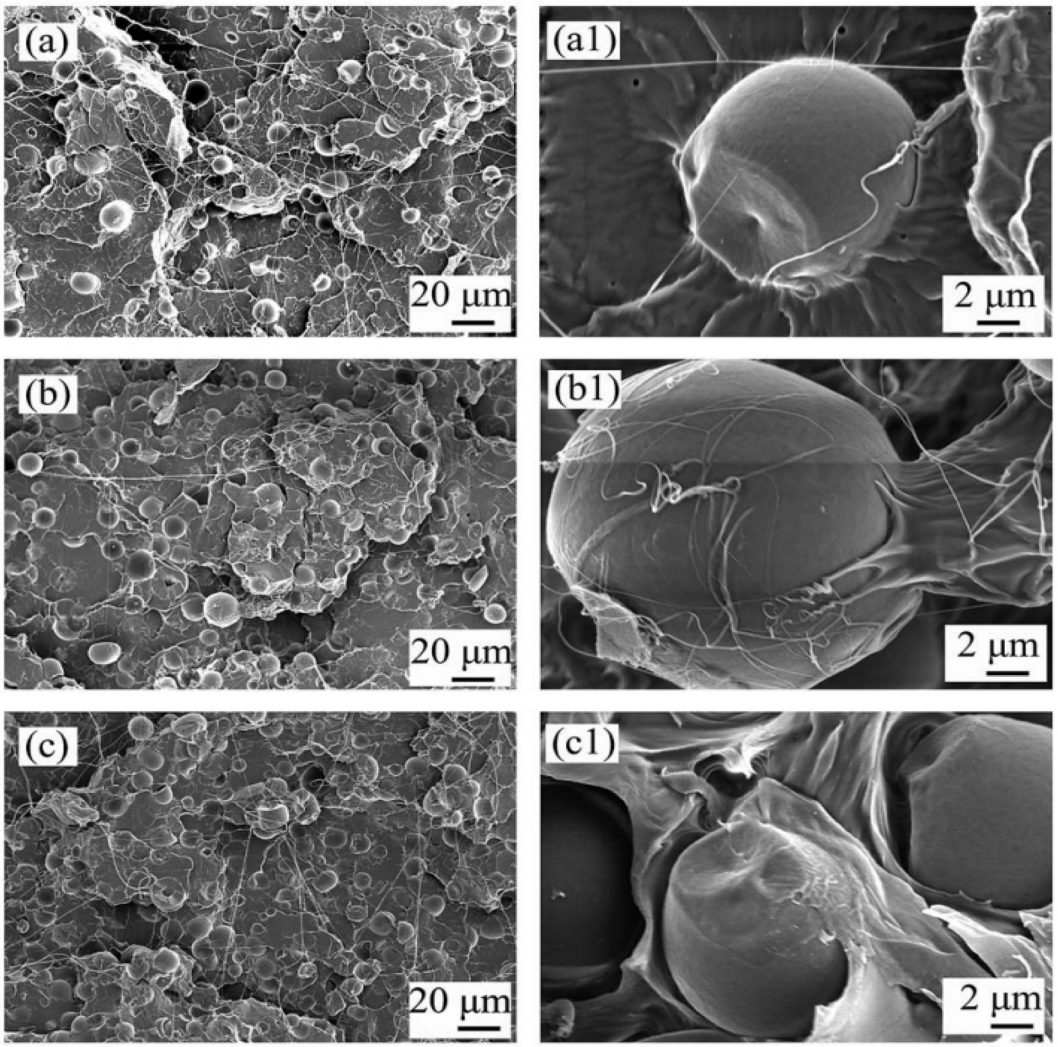

Fig. 6 SEM images of the cross sections of PLA/nGO@starch10 (a and a1), PLA/nGO@starch20 (b and b1), and PLA/nGO@starch30 (c and c1) after tensile breakage. ($T = 25$ °C)[193]

matrix. ΔH_m results here show that there is a link between compatibility and crystallizability and that the coating of stearic acid on the GO particles can enhance both.

Using DSC analysis, Valapa *et al.*[157] observed in Fig. 11 that the addition of graphene to the PLA matrix increased the melt temperature T_m and that T_g did not change compared to pure PLA. In addition, by increasing graphene to 03, the percentage of crystallinity increases. At higher amounts of graphene, the crystallinity percentage decreases, which is probably due to the poor accumulation and dispersion of graphene in the PLA matrix. Improving PLA crystallization by adding graphene is due to the presence of smaller graphene plates, which can facilitate the crystallization process of PLA.

Zhang *et al.*[188] using DSC images for pure asynchronous crystallization of pure PLA and PLA-ODAG nanocomposites observed that the addition of ODAG could reduce the cold crystallization temperature of T_C. The presence of ODAG increases the cold crystallinity of PLA, which is probably due to the effective nucleation effect of ODAG for Taylor PLA. Limitation of increased PLA crystallization at high ODAG values of more than 0.6 wt% may be due to ODAG accumulation, which reduces the number of nucleating sites. T_m and T_g are almost unchanged from pure PLA.

Huang *et al.*[82] examined the Taylor behavior of PLA GONS nanocomposites. They observed that at the beginning of melting an endothermic peak appears, which is the peak of 625 °C, which corresponds to T_g for pure PLA, which is probably short due to its regular structure. Adding GONS affects cold crystallization. Increasing the GONS rate decreases the peak height at low temperatures, but increasing the altitude indicates that the crystals are larger and a melting mechanism is formed due to the heterogeneous nucleation of the GONS.

Kuang *et al.*,[189] using the DSC curves (Fig. 12), no cold crystallization peak was observed for pure PLA and the melting peak was weak, but when the GO returned the cold Taylor temperature of the T_C increased, indicating that the scattered GO plates were due to the nucleation effect. They cause crystals. At 1% by weight the crystallization is reduced due to the effect of GO accumulation.

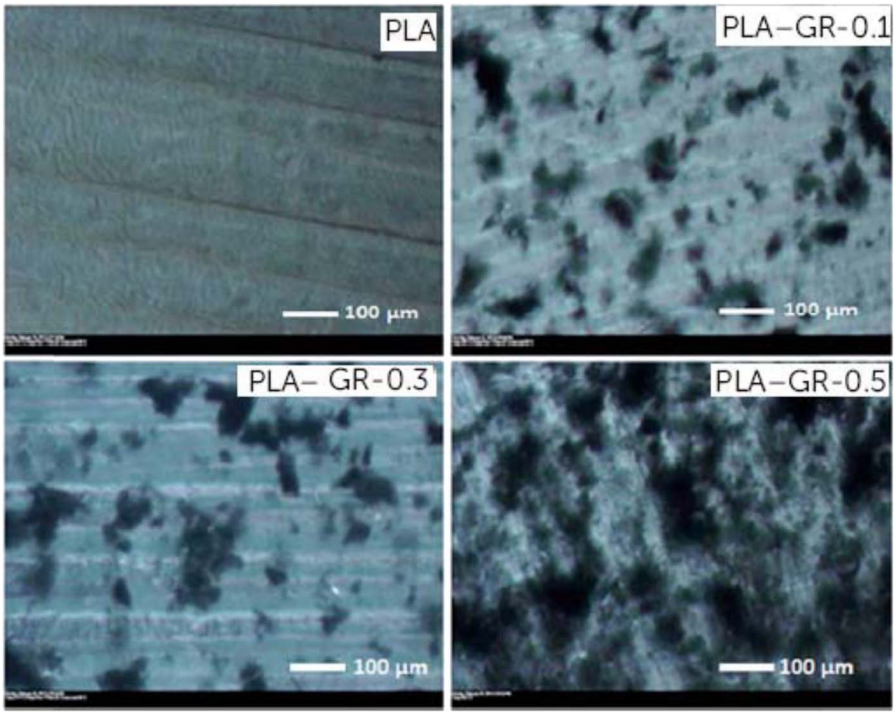

Fig. 7 Uniform distribution of graphene particles in the PLA matrix using a light microscope ($T = 25$ °C).[157]

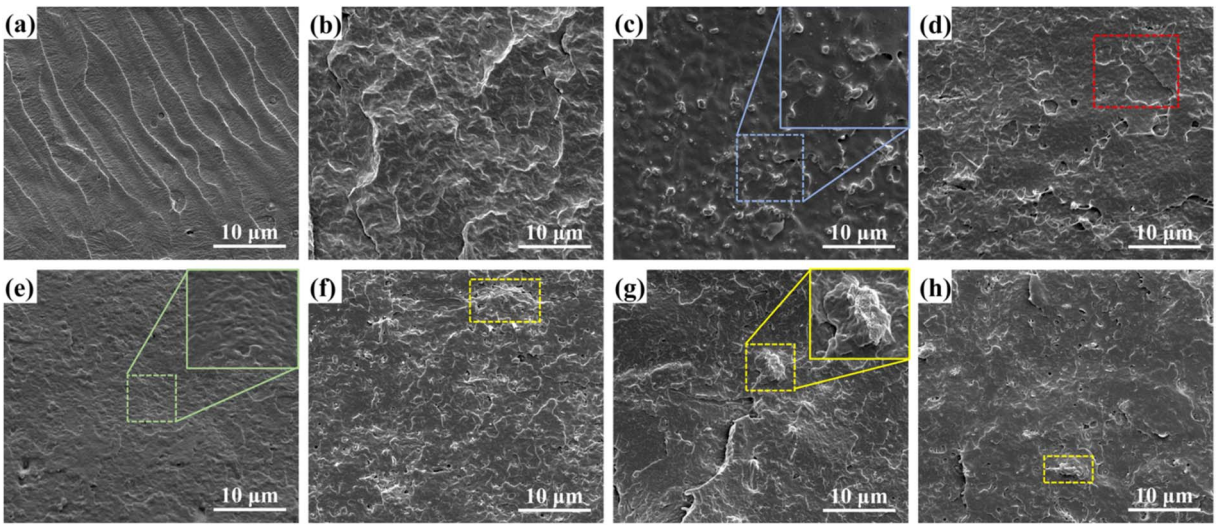

Fig. 8 SEM images for cryo-fractured surfaces of the (a) neat PLA, (b) neat PBS, (c) pristine PLA/PBS (90/10) blends, (d) PLA/PBS/MFCEPI (90/10/1), (e) PLA/PBS/MFC-EPI (90/10/2), (f) PLA/PBS/MFC-EPI (90/10/3), (g) PLA/PBS/MFC-EPI (90/10/4), and (h) PLA/PBS/MFC-EPI (90/10/5) ($T = 25$ °C) (this figure has been adapted from ref. 194 with permission from ACS, copyright 2020).

Kim and colleagues,[190] using the DSC analysis, found that increasing the amount of GO increases T_g, which this amplifying effect may lead to small mobility of PLA chain molecules. Graphene nanofibers as a nucleating agent increase the crystallization rate.

Rhim *et al.*[70] studied the effect of PLA film fabrication method on the thermal behavior and crystallization of the sample. According to Fig. 13, he observed that the T_g and T_c values of PLA films prepared by the solvent casting method are much lower than the corresponding values in the thermal compression method. The reduction of T_g of PLA films of solvent casting is related to the softening effect of the solvent. Such a decrease in T_g explains the changes in the mechanical properties and permeability of PLAs produced by the solvent method. In general, the mechanical properties and permeability of polymers are affected by T_g to any particular degree.

Zhao *et al.*[192] the melting temperatures of the two composites were both slightly lower than those of pure PLA. The crystallinity of the composites was also lower than that of pure PLA.

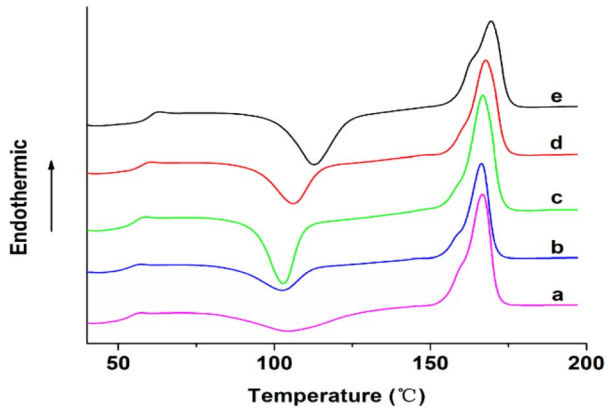

Fig. 9 DSC thermograms of (a) PLA; (b) PLA/15%nHA; (c) PLA/15% nHA-1%GO; (d) PLA/15%nHA-2%GO and (e) PLA/15%nHA-3%GO.[195]

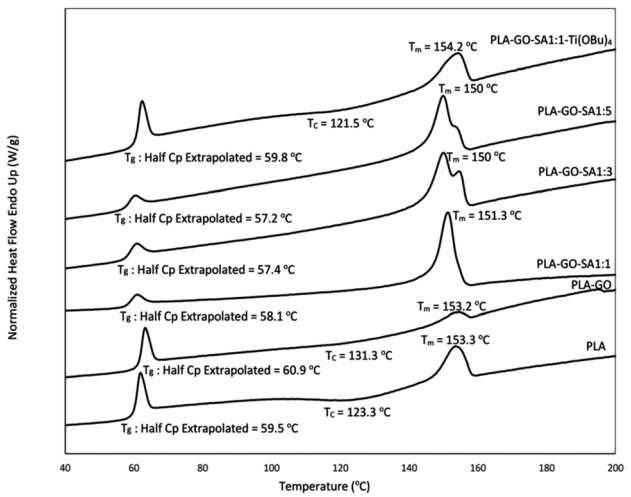

Fig. 10 DSC thermograms of PLA, PLA-GO, and PLA-GO-SA films (this figure has been adapted from ref. 62 with permission from Wiley, copyright 2015).

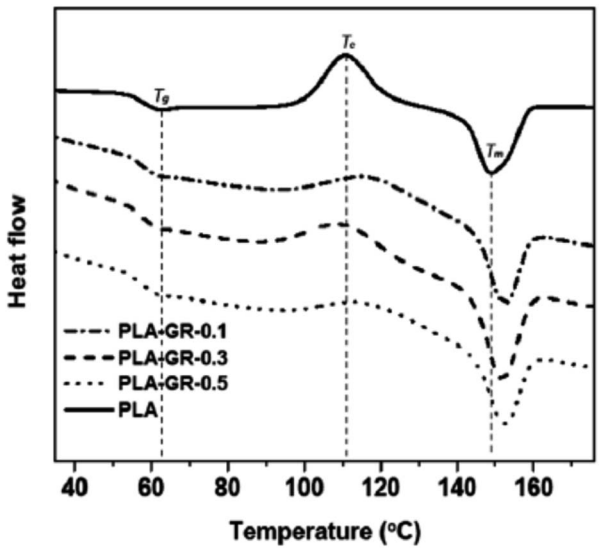

Fig. 11 DSC test results for PLA-Gr nanocomposites.[157]

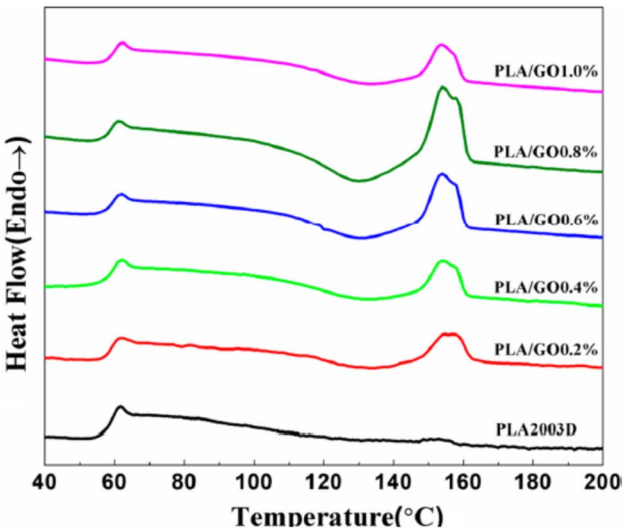

Fig. 12 DSC images for pure PLA and PLA-G0 nanocomposites (this figure has been adapted from ref. 189 with permission from ACS, copyright 2014).

Lim *et al.*[69] did not observe any peak of cold crystallization for the pure PLA sample due to the low crystallization rate of the PLA. In other words, at the applied cooling rate, the chains did not have the opportunity to crystallize and form crystals. By adding graphene nanoparticles, a peak of crystallization was observed, which means induction of crystallization with graphene particles in PLA. The main reason for this phenomenon is the increase in heterogeneous nucleation.

6.3. Spherolite growth behavior

Zhang *et al.*[22] using the POM images found that the addition of graphene significantly affected the morphology of the spherolite, the size of the spherolite decreased with increasing graphene, and graphene acted as a nucleating agent.

Patel *et al.* investigated[196] the crystallization behavior and spherulitic morphology of the neat polymers and their blends using POM, with the results shown in Fig. 14. Their result shown that the PLA shows no spherulites (Fig. 14a) under the given conditions, confirming the amorphous structure of the PLA. In contrast, the PHB film exhibited a crystalline phase (Fig. 14e) with large spherulites with a diameter of approximately 1 mm grown in helical strands radiating from the nucleation point. For the blends, mixing of PLA and PHB resulted in the formation of smaller spherulites, except for the 90 : 10 blend (Fig. 14b), where the blend did not show any spherulites, possibly due to the low PHB content that is insufficient to produce spherulites. The 75 : 25 blend shown in (Fig. 14c) demonstrates many very small spherulites (≤8 μm) that are well-dispersed in the matrix, whereas the 50 : 50 blend (Fig. 14d) has a larger spherulite size (≤46 μm) and forms

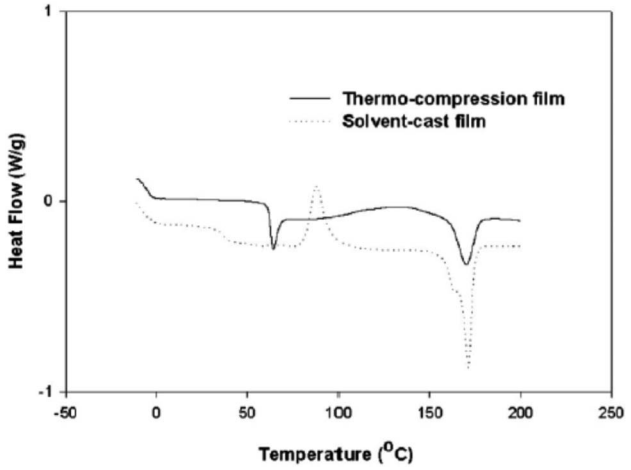

Fig. 13 DSC curve of PLA films prepared by solution methods and thermal compression (this figure has been adapted from ref. 70 with permission from Wiley, copyright 2006).

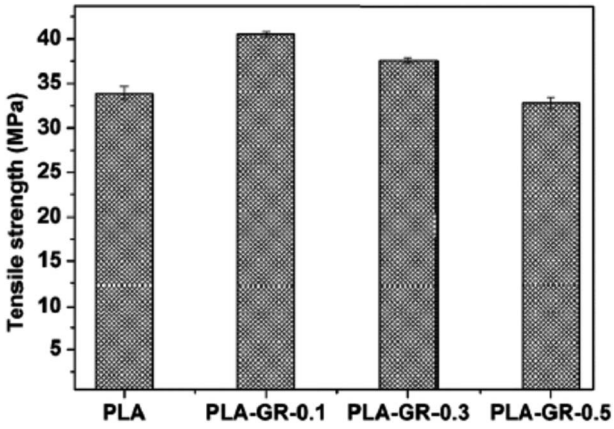

Fig. 15 Changes in yield strength in terms of graphene nanoparticles ($T = 25$ °C).[157]

a continuous phase. This finding shows that the size of spherulites increased with the amount of PHB present in PLA. The formation of a large number of relatively small spherulites in the 75 : 25 blend may be ascribed to the number of nucleation sites of the spherulites that is high enough to obstruct the growth of large spherulites.

To demonstrate the greater nucleation effect of ODAG on PLA crystallinity, Zhang *et al.*[188] investigated the isothermal crystalline morphology of pure PLA and its nanocomposites at 120 °C with POM. They observed that, for example, pure PLA, the size of the spherolites is relatively large, and with the addition of ODAG, the number of spherolites increases significantly and their size decreases. The morphology of the spherolite clearly confirms the nucleation effect of ODAG with DSC results.

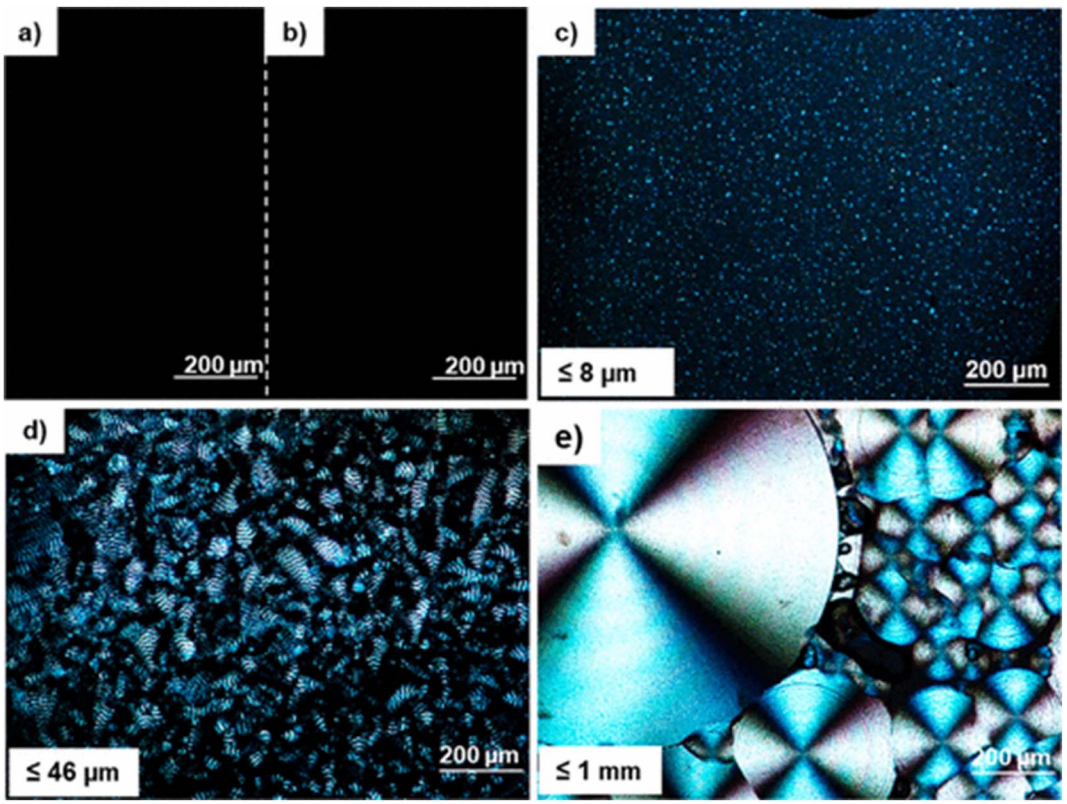

Fig. 14 Polarized optical micrographs of melted films on the hot stage showing the crystallization of (a) pure PLA, (b) 90 : 10 with no visible crystallization, (c) 75 : 25 small crystallites well-dispersed in the PLA matrix, (d) 50 : 50 with large spherulites, and (e) pure PHB showing very large spherulite size compared to the blends. ($T = 90$ °C) (this figure has been adapted from ref. 196 with permission from ACS, copyright 2022).

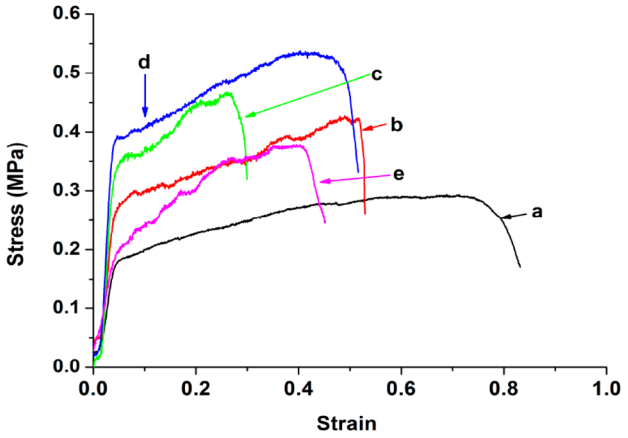

Fig. 16 Study of stress–strain diagram (T = 25 °C).[195]

6.4. Mechanical properties

Improving the mechanical properties using nanoparticles is completely dependent on the amount of nanoparticles added. Chartarrayawadee *et al.*[62] investigated the effect of GO and SA bonding on mechanical properties, tensile strength, elongation and modulus for specimens. They observed that the addition of GO alone did not have a significant effect on the tensile strength of pure PLA, instead the addition of stearic acid increased the tensile strength. Sample 1 : 1 PLA-GO-SA has the highest tensile strength due to the improved compatibility of GO with PLA due to SA alkyd hydromatic chains. In Fig. 15, Valapa *et al.*[157] observed the highest tensile strength and elongation at 0.1-PLA-Gr composite by performing a tensile test. However, with increasing amount of graphene, tensile strength and elongation had a decreasing trend due to the accumulation of graphene particles and their agglomeration.

Chen *et al.*,[195] according to Fig. 16, observed that pure PLA film behaves normally brittle, while nanocomposite film shows soft failure behavior. The results show that PLA is strengthened and strengthened by oxide (GO) and a nano hydroxyapatite rod (nHA). Due to the structure between the filler surface and the matrix; Young's modulus and tensile strength increase and elongation decrease. Under tensile loading, an interfacial reaction takes place between GO and PLA, causing fuzzy separation. This fuzzy separation not only increases the deformation energy for failure, but also causes the brittle transition to softness and crack deflection. After tensile testing, the specimens have completely different failure levels. The increase in modulus and strength with GO values from 0–3% by weight is significant.

Huan *et al.*[197] observed in Fig. 17 that the tensile strength during fracture and the tensile modulus improved with increasing nanocarbons. The combination of graphene nanofibers reduced elongation at break. Due to the elongation properties of the nanocomposite prepared in this study, it is suitable for packaging.

Rostami *et al.*[198] the mechanical properties of PLA, PLA + GnPs and CNTs were evaluated using tensile tests. Fig. 18 plots

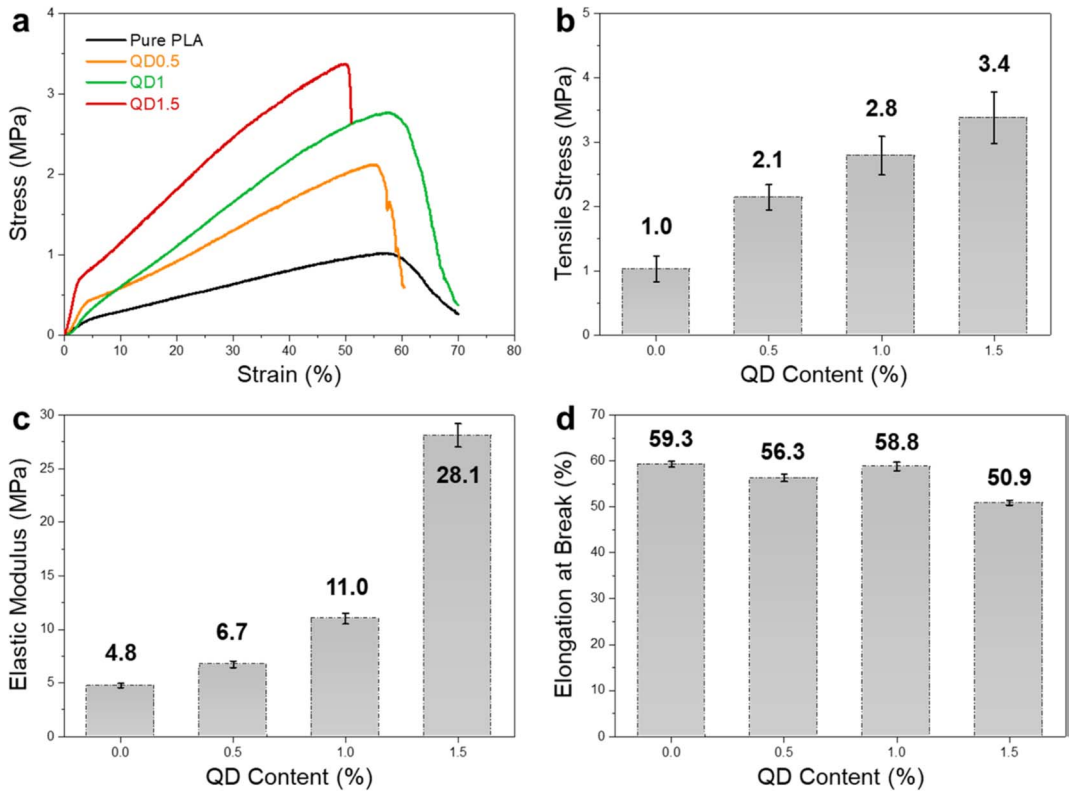

Fig. 17 Tensile behavior of electrospun PLA/QD membranes. (a) Typical stress–strain curves for the composite membranes. (b) Tensile stress, (c) elastic modulus, and (d) elongation at break as a function of QD loadings. The average values and error bars are marked. (T = 25 °C) (this figure has been adapted from ref. 197 with permission from ACS, copyright 2021).

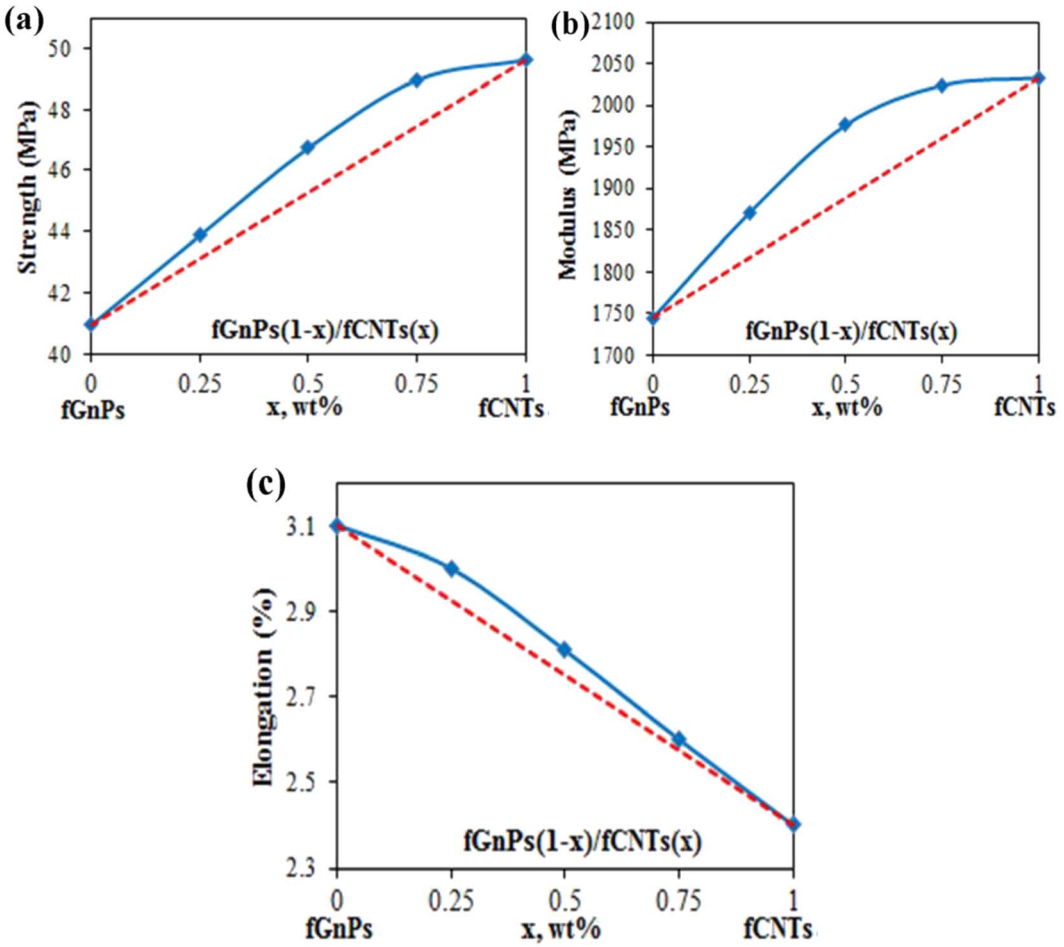

Fig. 18 (a) Tensile strength, (b) tensile modulus and (c) elongation at break of hybrid filler nanocomposites with different fGnPs:fCNTs ratios at overall concentrations of 1 wt% (T = 25 °C).[198]

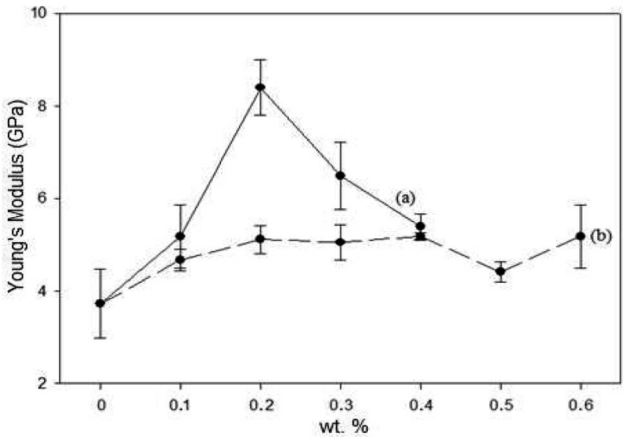

Fig. 19 Young's modulus of composite with various filler contents (a) CNC and (b) GO (T = 25 °C).[191]

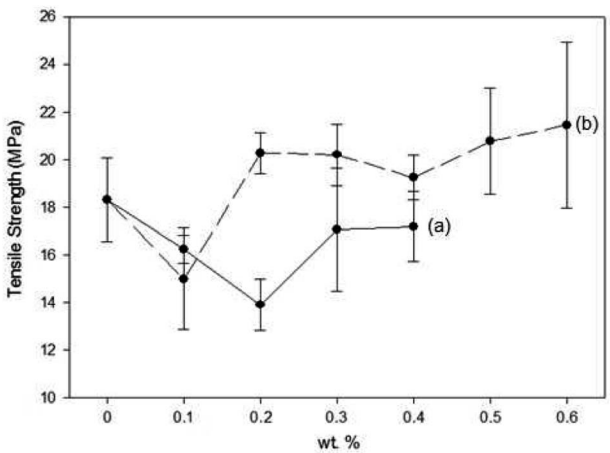

Fig. 20 Tensile strength of composite with various filler contents (a) CNC and (b) GO (T = 25 °C).[191]

the tensile modulus and strength, and the fracture strain of the hybrid filler nanocomposites as a function of the mix ratios at the overall filler concentrations of 1 wt%. The hybrid filler nanocomposites show a positive deviation in the tensile modulus and strength when compared with the mixture law (the dashed line).

The effect of graphene oxide content on the mechanical properties of PLA was studied by Chan *et al.*[191] It is clear that the

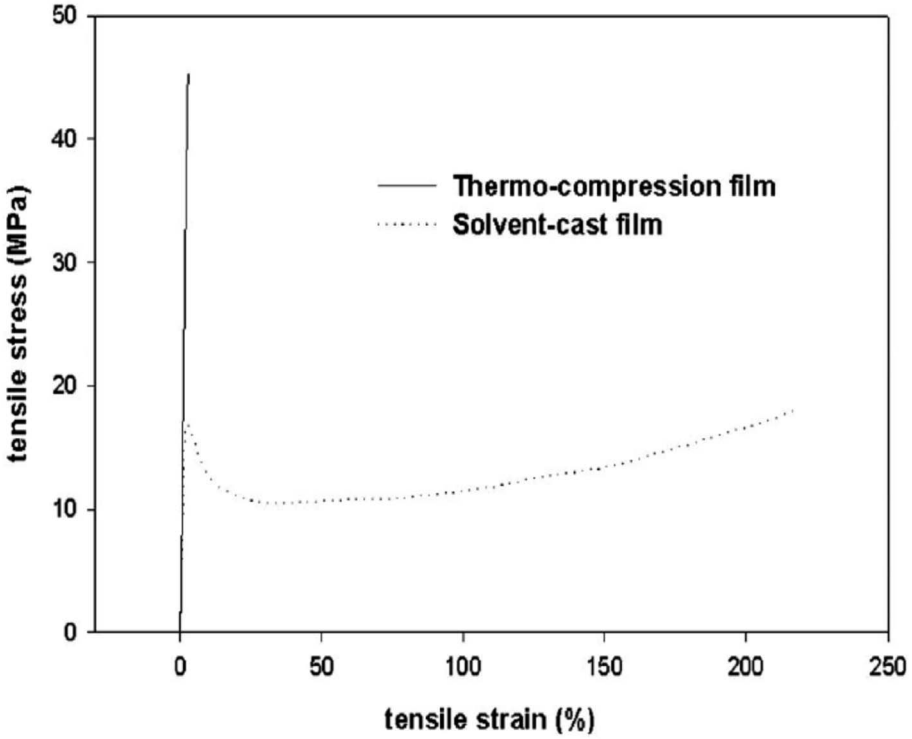

Fig. 21 PLA stress–strain curve ($T = 25$ °C). (This figure has been adapted from ref. 70 with permission from Wiley, copyright 2006).

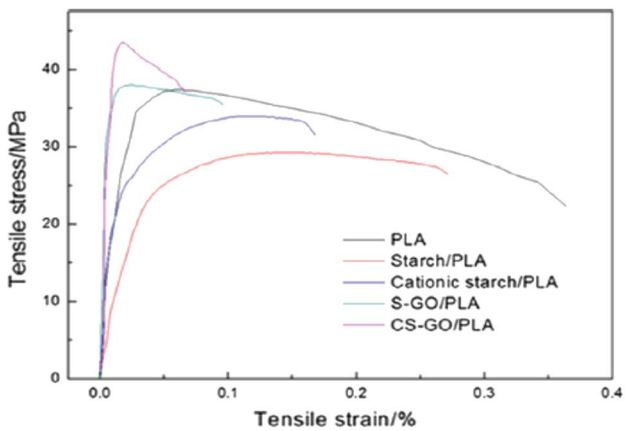

Fig. 22 Strain stress curve ($T = 25$ °C) (this figure has been adapted from ref. 199 with permission from Elsevier, copyright 2015).

changes in yield stress and Young's modulus are not uniform and decrease first and then increase. The results of this study can be seen in Fig. 19 and 20.

Rhim *et al.*[70] compared PLA films prepared by heat-compression method and solution method. Fig. 21 shows the stress–strain curve of pure PLA produced by these two methods. According to the diagram, it is quite clear that with the heat-compression method, the yield stress and strength of the material increase, but the stiffness of the material decreases.

In Fig. 22, the stress–strain curves of Nuona *et al.*[199] obtained pure PLA, starch and PLA, starch and graphene oxide, and PLA and observed that the CS-GO/PLA composite had the highest strength because graphene oxide acts like a bridge for PLA and starch bonds.

6.5. Thermal properties

Rostami *et al.*[198] investigated the thermal stability of PLA-GR nanocomposites, which in Fig. 23 they observed improved by adding graphene to the pure sample.

Using TGA analysis, Valapa *et al.*[157] found that the main process of thermal degradation of PLA begins mainly at temperatures above 300 °C, which is mainly attributed to the esterification of the transformer (discontinuity reaction). The results in Fig. 24 clearly show that the 0.5-PLA-GR composite improves thermal stability over pure PLA by about 6 °C.

Huang *et al.*[82] used TGA to study the thermal stability of pure PLA and GONS nanocomposites. Fig. 25 shows that strong adhesion between the GONS and the PLA matrix can limit the mobility of the PLA chain in the vicinity of the GONS surface, resulting in excellent thermal stability of the PLA matrix.

Kim *et al.*,[183] using TGA analysis, observed in Fig. 26 that thermal stability increases with increasing GO value.

6.6. Optical transparency

Minimizing optical transparency is important in the development of the packaging industry by increasing the gas impermeability performance. Photochemical degradation of plastic occurs when exposed to high energy UV-B radiation. Valapa *et al.*,[157] by examining a wavelength range of 700–200 nm in Fig. 27, observed that for pure PLA film, 72% of the light

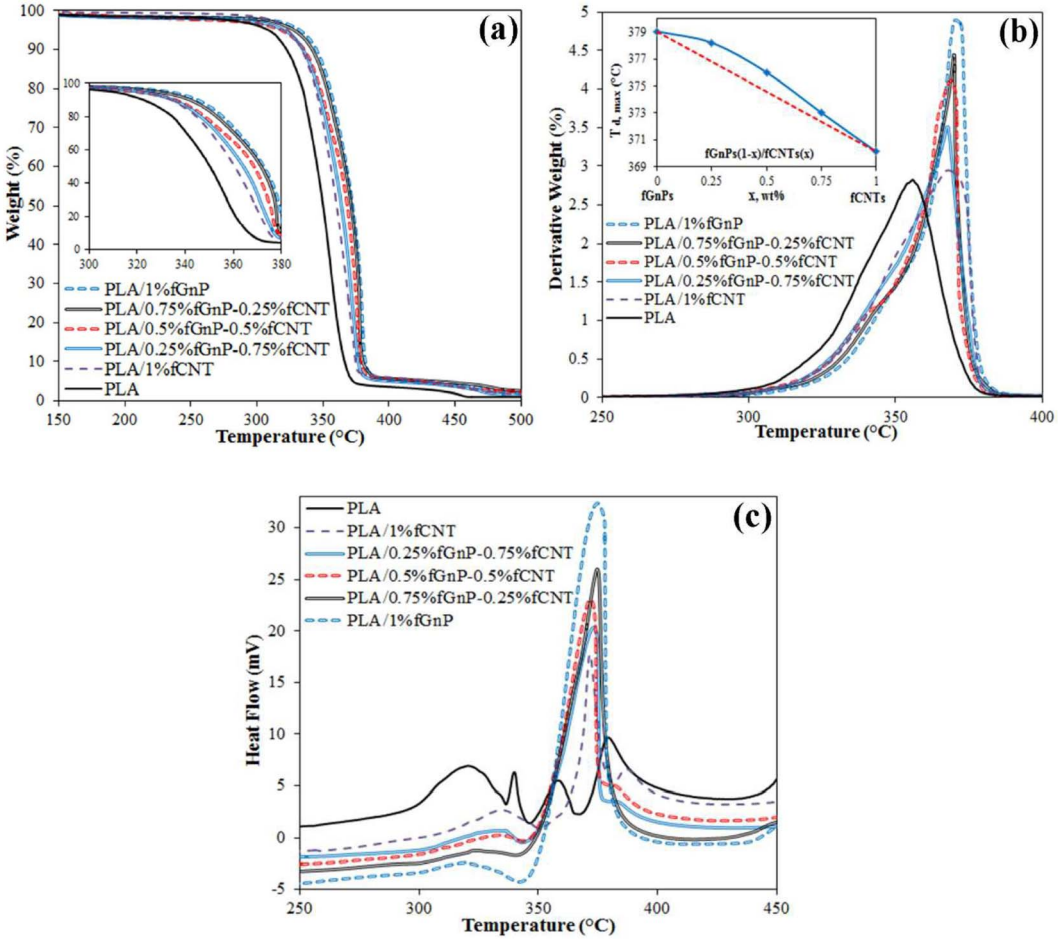

Fig. 23 (a) TGA, (b) DTG, and (c) DTA curves diagram for pure PLA and different amounts of graphene.[198]

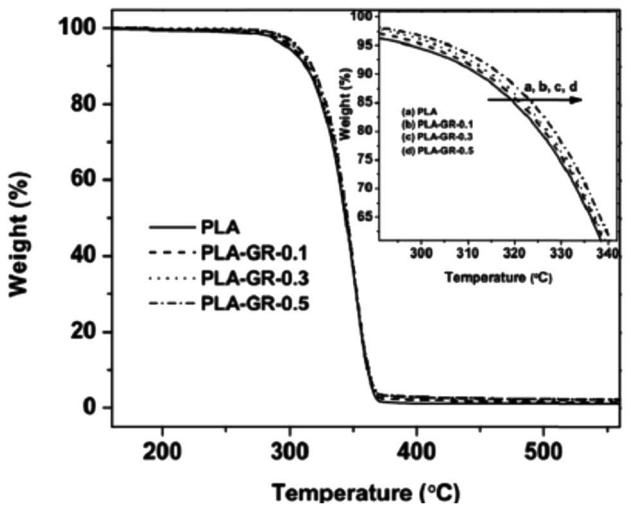

Fig. 24 TGA diagram for pure PLA and its nanocomposite sample with different amounts of graphene.[157]

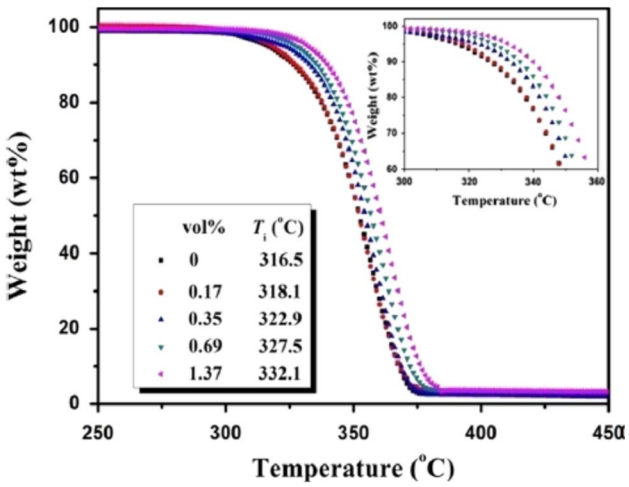

Fig. 25 TGA diagram of pure and nanocomposite PLA samples with different GONS values (this figure has been adapted from ref. 82 with permission from Elsevier, copyright 2014).

transmission occurs. After adding graphene to the PLA matrix, the transparency of PLA films decreased. The highest degree of transparency was observed for 0.5-PLA-GT nanocomposite film.

The transparency of PLA and nanocomposites of PLA and graphene oxide as well as PLA and graphene nanosheets (GNP) has been investigated in ref. 86. In this study, it was observed

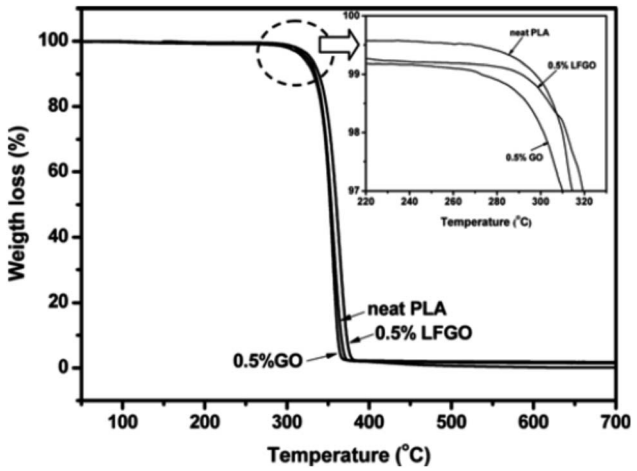

Fig. 26 TGA diagram of pure and nanocomposite PLA sample with 0.5% by weight of graphene oxide (this figure has been adapted from ref. 183 with permission from ACS, copyright 2008).

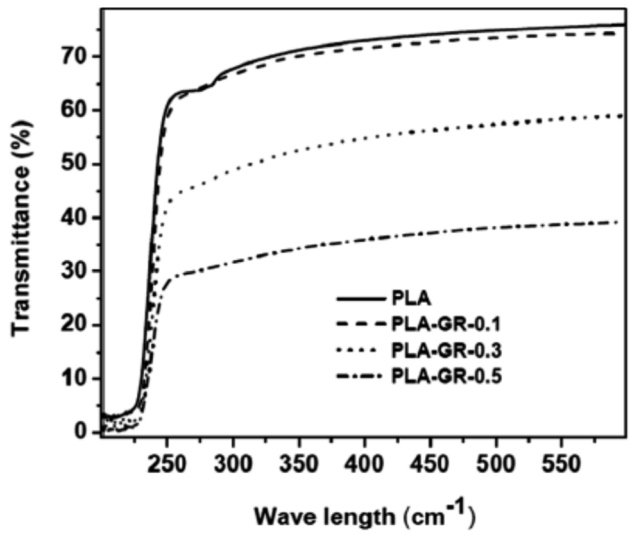

Fig. 27 Optical transparency image of PLA and PLA-Graphene nanocomposite (T = 25 °C).[157]

that with increasing filler, the samples become duller. Graphene oxide also has a higher transparency than graphene nanosheets. The transmittance of samples: PLA = 92, GO 0.2 wt% = 81, GO 0.4 wt% = 76, GO 0.6 wt% = 72, GNP 0.2 wt% = 55, GNP 0.4 wt% = 24, GNP 0.6 wt% = 23.

In a study by Huang *et al.*,[82] the percentage of light passing through PLA and PLA/GONS nanocomposites was obtained in terms of UV wavelength (Fig. 28). As the wavelength increases, the light transmitted through pure PLA increases, while for PLA/GONS nanocomposites the light transmittance changes are very small in terms of wavelength.

Kim *et al.*[183] investigated the possibility of using graphene oxide nanocomposite films in food packaging film and evaluated the degree of optical transparency. They observed that the addition of GO reduces the transparency of the nanocomposite film due to the increase in light scattering. Its photo can be seen in ref. 174.

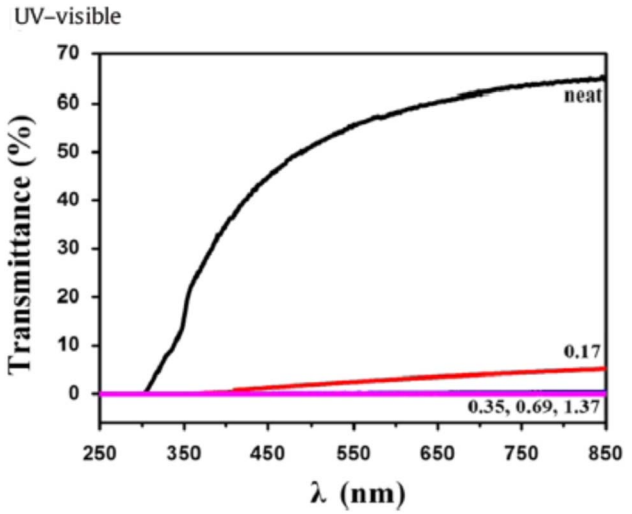

Fig. 28 Percentage of light passing through PLA and PLA/GONS nanocomposites in terms of UV light wavelength (T = 25 °C) (this figure has been adapted from ref. 82 with permission from Elsevier, copyright 2014).

6.7. Rheological properties

To investigate the effect of GO on rheological properties, Kuang *et al.*[189] measured and analyzed the storage modulus (G′), the loss modulus (G″), and the complexity viscosity (η^*) and observed that G′ and G″ were higher in PLA/GO nanocomposites. It is pure PLA and increases with increasing amount of GO. Differences in low-angle frequencies increase the elasticity of PLA/GO nanocomposites relative to pure PLA due to the amplifying effect of GO nanofiller, which forms networks bonded to a polymer matrix. The log G' *versus*' log G'' is also shown in Fig. 29. The slope of this curve is almost indicative of the isotropic and homogeneous properties of the polymer melt, and the transition and slope change means that a significant change in the structure of the composites has occurred. It can be seen that the slope of log G′ against' log G ′decreases with increasing value of GO, indicating that the composites have become more heterogeneous and also indicating that there has been a significant change in the structure of PLA/GO nanocomposites. The changes in complexity (η^*) viscosity of PLA and PLA/GO nanocomposites are also shown in Fig. 26. It can be seen that pure PLA and 0.2% PLA/GO show the typical Newtonian liquid pattern, η^* remains approximately the same at a wide range of angular frequencies. As the value of GO increases, η^* nanocomposites gradually decrease with increasing angular frequency. These results show that the addition of GO can gradually change the rheological behavior of nanocomposites from Newtonian liquid behavior to plastic-like liquid behavior.

6.8. X-ray diffraction spectroscopy

Wu *et al.*[193] investigated the crystal structure of PLA and PLA@starch and PLA/nGO@starch nanocomposites using X-ray diffraction. X-ray diffraction patterns PLA and PLA@starch and PLA/nGO@starch are shown in Fig. 30. In addition,

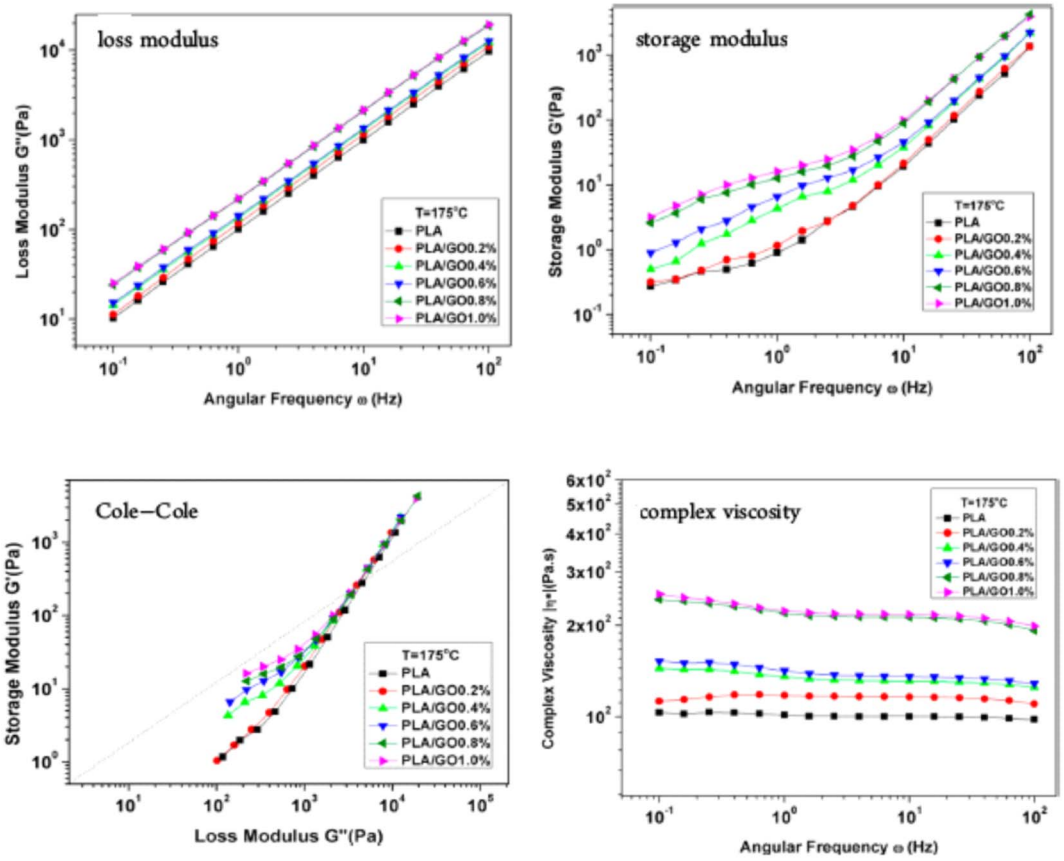

Fig. 29 Rheological properties of PLA and PLA/GO composites ($T = 175$ °C) (this figure has been adapted from ref. 189 with permission from ACS, copyright 2014).

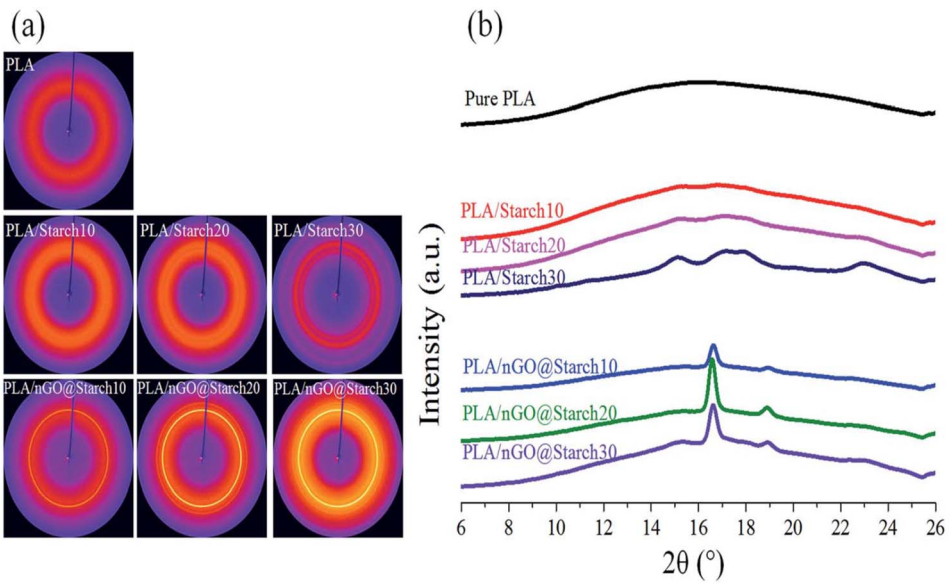

Fig. 30 2D-WAXD images (a) and 1D-WAXD intensity curves (b) of pure PLA, PLA/starch composites and PLA/nGO@starch composites; each composite type has a starch concentration of 10%, 20% and 30%.($T = 25$ °C).[193]

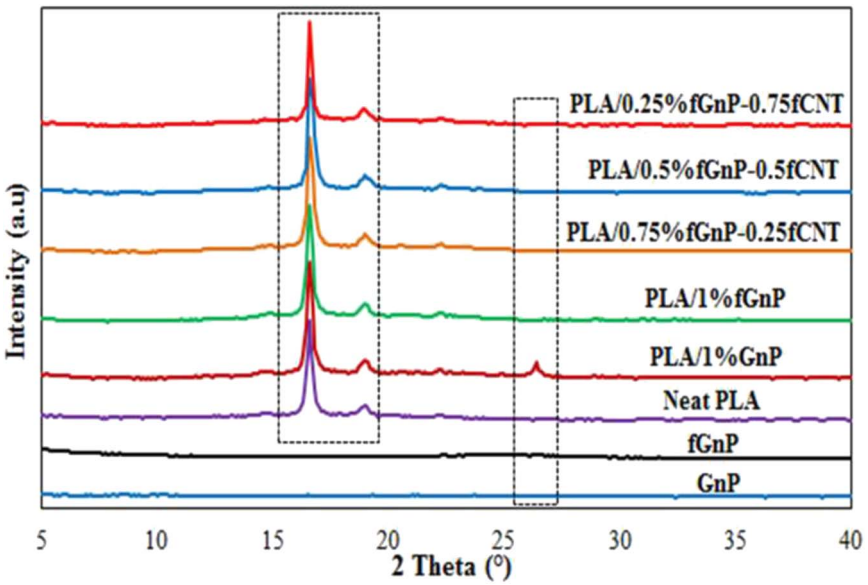

Fig. 31 Shows the XRD patterns of the pristine and functionalized GnPs, neat PLA, and single and hybrid nanofillers filled PLA (T = 25 °C).[198]

1D WAXD intensity profiles were extracted. As shown in Fig. 30a, a weak halo was shown in pure PLA and PLA/starch composites, indicating an almost amorphous PLA phase. This agrees with the 1D-WAXD curves, where only wide amorphous peaks were seen (Fig. 30b). It is interesting to note that PLA/starch30 exhibits several individual circles and shows weak signals in the 1D-WAXD curve. This should be due to the higher concentration of starch, which provides the crystalline structure and attributes to the sharp peak. For the composites containing nGO, circles appeared and became clearer with increasing concentrations. Two distinct diffraction peaks were observed and were typically located at 2θ = 16.7° and 19.0°. These peaks are assigned to the lattice planes (200)/(110) and (203) of the a-crystal form of PLA.

Kim *et al.*[190] also studied the structural properties of PLA and PLA/Gr nanocomposites using the patterns created in XRD. By comparing the obtained results with the XRD pattern of pure graphite, a change in the structure of the molecules in the

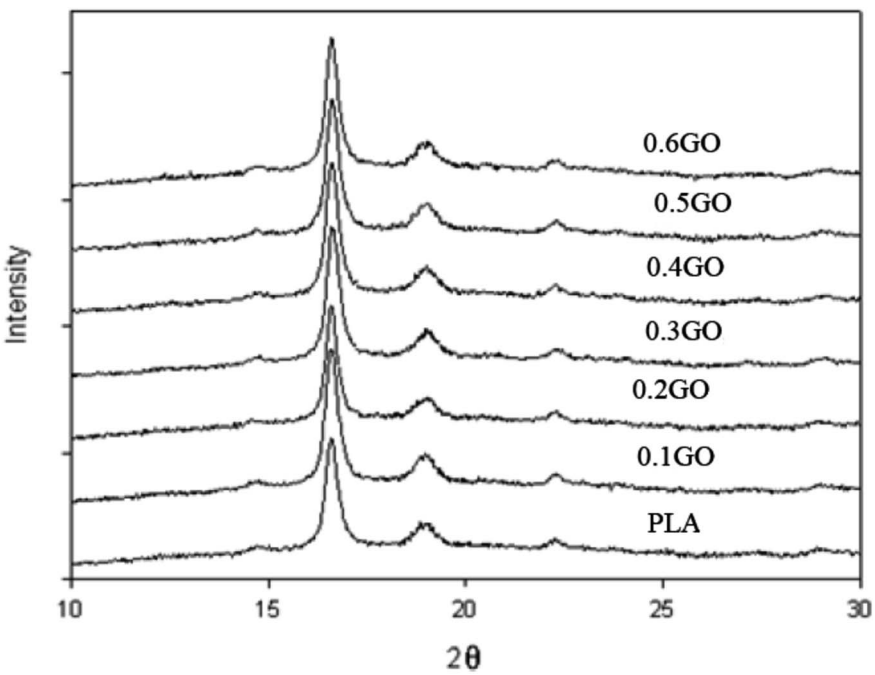

Fig. 32 XRD pattern of PLA material and PLA/GO nanocomposites (T = 25 °C).[191]

nanocomposites has been observed. The marked PLA peaks are shown in Fig. 31, $2\theta = 16.3$, 19.1, and 26.4. Fig. 31 shows the XRD patterns of the pristine and functionalized GnPs, neat PLA, and single and hybrid nanofillers filled PLA.

Ref. 191 also shows XRD patterns of PLA and PLA/GO nanocomposites in Fig. 32. He observed that the peaks in nanocomposites are in the range of about 3% compared to pure PLA, which may be due to the very small amounts of fillers.

6.9. The effect of UV rays on the properties of polymers

No research has been done on the effect of UV radiation on the properties of PLA/Gr nanocomposites or on PLA polymer. The following are some studies on other polymers. Oluz *et al.*[200] investigated the effect of UV rays on the mechanical properties and degradation of polyethylene and observed that the addition of vanadium acetone, serpentine and Cloisite 30B accelerates the reduction of elongation with increasing time. Nikafshar *et al.*[201] also studied the effect of UV radiation on the rate of degradation and mechanical properties of epoxy resins and observed that with exposure to UV for 800 hours, yield stress of 30%, refractive index of 36% and Young's modulus of about decreased by 1%.

6.10. Thermophysical properties as function of temperature

Giovanni Spinelli *et al.*[202] examined experimental and simulation studies of temperature effect on thermophysical properties of graphene-based polylactic acid. Fig. 33 from (a) to (c) (3D view on the left and 2D graphics on the right) depict the thermal conductivity (l), the thermal diffusivity (a), and specific heat capacity (C_p) as a function of GNPs content and of the temperature in the range between 298.15 and 373.15 K. More in detail, Fig. 30a shows the comparison of the thermal conductivity of all samples. A clear increase in thermal conductivity with increasing filler content is observed. In fact, at the temperature of 298.15 K, the thermal conductivity for the pure PLA is 0.173 W m K^{-1}, whereas for PLA with 6 wt% of GNPs reaches the value of 0.470 W m K^{-1}, which corresponds to a significant improvement of about 171%.

Therefore, since classical thermally insulating materials show a thermal conductivity of the order of 10^{-3} (W m^{-1} K^{-1}), the proposed nanocomposites, in light of the measured values of conductivity and in combination with the other benefits typical of polymer materials, can be considered suitable for potential heat transfer applications.

With reference to the temperature influence, the thermal conductivity increases slightly as it increases, at least in the

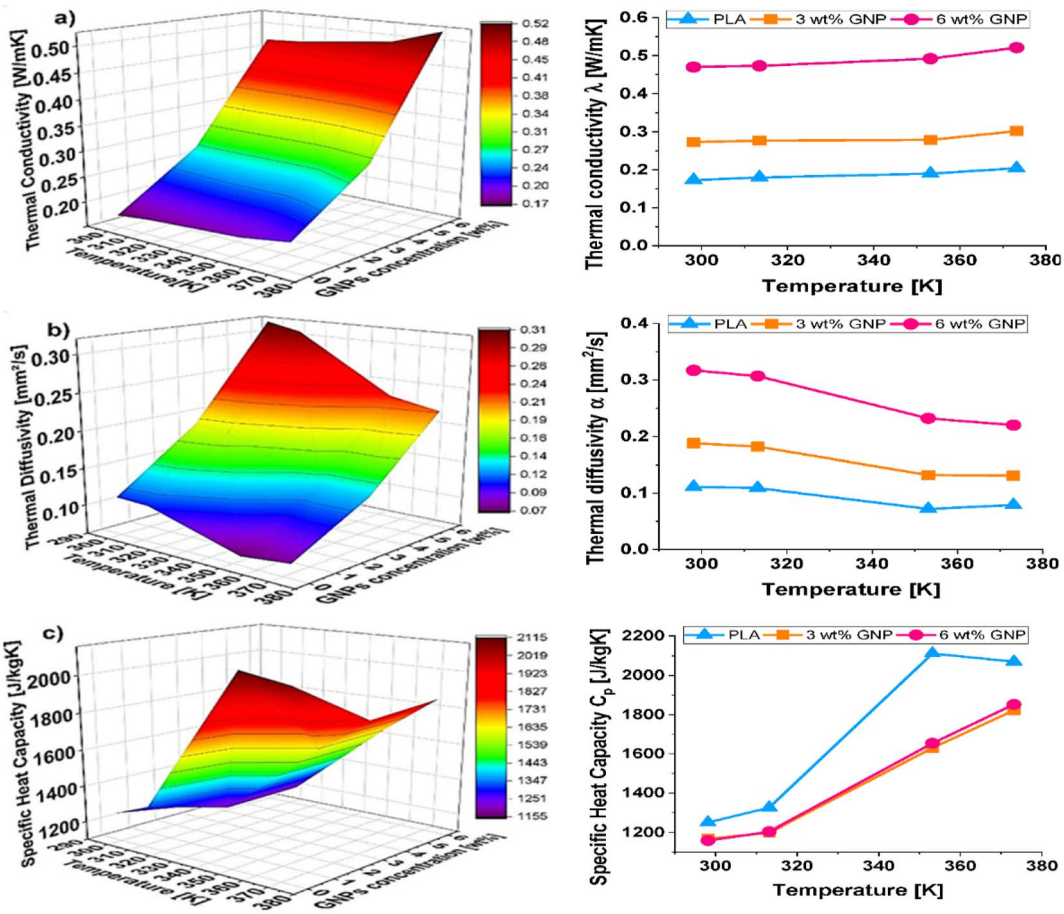

Fig. 33 Comparison of thermophysical properties of pure PLA, PLA filled with 3 wt% GNPs and PLA reinforced with 6 wt% GNPs in terms of thermal conductivity (λ), thermal diffusivity (α), and specific heat capacity (C_p) in (a–c), respectively.[202]

investigated temperature range. This is because, with increasing temperature, the molecular vibrations increase, thus leading to a higher phonon propagation and hence to a higher thermal conductivity.

However, the temperature has a great impact on the thermal conductivity of nanoreinforced polymers due to different mechanisms such as scattering mechanism, changes in specific heat, polymer chain orientation, and so on. In brief, up to a certain temperature, these influencing parameters favor the thermal conductivity, which will start to progressively increase with the temperature. Differently, at higher temperatures, mainly due to the anharmonic scattering and changes in the molecular morphology, a balance (or also a worsening) between phonon propagation and its scattering is reached and, consequently, it is expected that the thermal conductivity reduces with temperature.

Differently, as can be noted from Fig. 30b, the thermal diffusivity decreases with increasing temperature. In particular, the change in slope between 313.15 and 353.15 K is caused by the glass transition (which is expected around 333.15 K). The glass transition is also indicated in the specific heat determination by a step (Fig. 33c). By comparing these trends all together (Fig. 33a–c), it is interesting to note how the temperature dependence for the conductivity, at least in the investigated range, presents a sweet profile that becomes slightly more marked for diffusivity, whereas it is clearly evident for the specific heat capacity.

Adesina, O. T., *et al.*[203] examined the influence of process parameters of Spark plasma sintering (SPS) technique on the densification and hardness properties of graphene (GNP) reinforced polylactic acid (PLA) nanocomposite. The numerical experiment was designed in accordance with response surface methodology (RSM) using central composite design (CCD). Five percent GNP were used as reinforcement in the polylactic acid matrix at varying conditions of temperature and pressure for the physical experiment. The validation of the developed model, as well as the effect of each variable and their interaction, was analyzed using the analysis of variance (ANOVA). Taking the material hardness and density as the response of the designed experiment, the data obtained from both the numerical and physical experiment were statistically analyzed to obtain a predictive model which correlates the hardness and density as a function of the independent process parameters.

They presented a quadratic model used to predict the density property of PLA/GNP nanocomposite as a function of temperature (A) and pressure (B), based on this model, the density decreases with increases temperature.

$$\text{Density} = 1.28 + 3.746 \times 10^{-3} \times T + 1.582 \times 10^{-3} \times \text{P}2.5 \times 10^{-4} \times \text{T} - 1.063 \times 10^{-3} \times T^2 + 4.375 \times 10^{-4} \times \text{P}^2$$

6.11. Effect of temperature on the rheological properties

Wang *et al.*[204] investigated the incorporation of graphitic nanofiller and poly(lactic acid) in fused deposition modeling. They presented research results showing that the property of fused

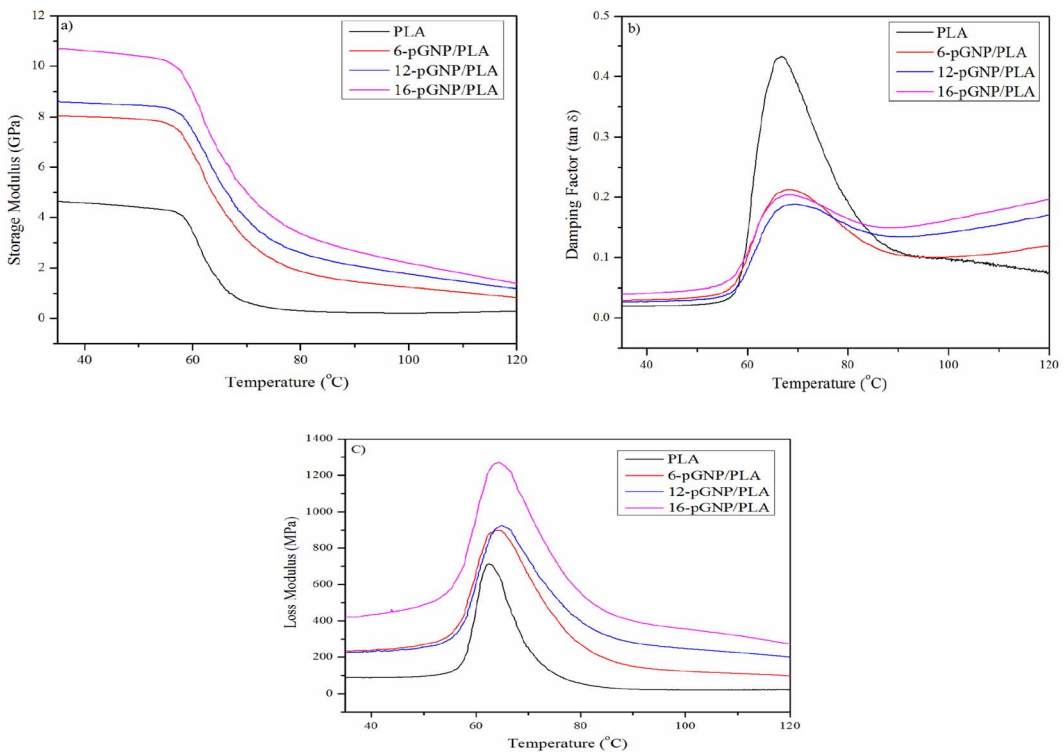

Fig. 34 Dynamic mechanical properties of neat PLA and pGNP/PLA nanocomposites as a function of temperature: (a) storage modulus, (b) loss factor, and (c) loss modulus.[205]

Table 2 Summarizes the results of the research conducted in some articles

Name	Year	Title	Result
Valpa *et al.*[157]	2015	The effect of graphene content on the properties of PLA nanocomposites	Gr acts as an effective nucleating agent in enhancing the behavior of Taylor PLA, improving thermal stability and reducing transparency. Provides tensile strength of PLA-GT composites for loading 0.1% by weight of GR, which indicates good adhesion of nanoparticles and the substrate
Chen *et al.*[87]	2011	The effect of graphene deposition time in chloroform on the structural and thermal properties of PLAG	Graphene can: reduce the mobility of polymer chains and has an inhibitory effect on the PLA crystallization process. It also leads to lasting improvement
Pinto *et al.*[9]	2012	Investigation of the effect of graphene oxide and graphene nanosheets on the mechanical properties and penetration of PLA gas	G0 increases the yield stress and the Young's modulus. Optimal load for mechanical performance at 0.4 wt% reduces permeability to oxygen and nitrogen
Huang *et al.*[82]	2014	Impact of graphene oxide nanofibers on the appearance and permeability of PLA gas	Due to the presence of GONS: Crystallization increased because they had a heterogeneous nucleation effect. Due to the excellent thermal stability of the PLA matrix. The variation of transmitted light is very small in terms of wavelength, almost no ultraviolet light can penetrate. The permeability coefficient of O2 and CO2 is reduced
Kuang *et al.*[189]	2014	Investigation of structural and rheological properties of PLA/GO foams	The cold crystallization temperature T rises. G′and G″ in PLAGO nanocomposites are higher than specific PLA and increase with increasing GO value. Adding GO can gradually change the rheological behavior of nanocomposites from Newtonian liquid behavior to plastic-like liquid behavior
Chartarrayawadee[62]	2017	Use of stearic acid to improve the mechanical properties of PLAGO	Addition of stearic acid has a softening effect, increases the compatibility of GO particles with PLA matrix, which leads to nucleation effect, as well as increasing tensile strength and elongation and modulus. The presence of ODAG increases crystallinity due to effective nucleation effect
Zhang *et al.*[192]	2015	Investigation of the effect of operating graphene on the structural and mechanical properties of PLA	By mixing 0.4% by weight of ODAG, the Young's modulus and tensile strength increase and elongation decrease. Apples become thicker in the sample. Improves thermal stability

deposition modeling (FDM) products is obtained jointly by careful control of processing parameters, structure of products, and the composition of material. In this manuscript, poly(lactic acid) (PLA) was incorporated with graphene or carbon nanotube (CNT) through repeated melt blending. Filament of the PLA/graphitic nano-filler was prepared and used in FDM. Rheological and thermal analysis were conducted to assess the suitability of the composite as FDM feedstock, and mechanical and electrical property were tested subsequently. Research results show that viscosity decreases with increasing temperature. The research results can be seen in ref. 153.

Zhang, Qi *et al.*[205] fabricating and characterizing multifunctional graphene nanoplatelets-based polylactide nanocomposites and investigated their properties including morphological, surface-chemical, mechanical, and thermo-mechanical properties. They showed increase in tensile modulus as compared to that of PLA. Storage modulus and glass transition temperatures of the PLA/GO nanocomposites were much higher than those of PLA as shown in Fig. 34.

6.12. Effect of temperature, humidity and UV on the aging of PLA and composites

Manish Kumar Lila *et al.*[206] investigated accelerated thermal ageing behavior of bagasse fibers reinforced poly(lactic acid) based biocomposites. Specimens of iocomposites were fabricated and exposed to temperature cycles of −20 °C and 65 °C (12 hours each) for 12 weeks and characterized after every 4 weeks of exposure. Tensile and flexural properties exhibited steady improvement on exposure up to 8 weeks, followed by a reduction after ageing for 12 weeks.

Rocca-Smith *et al.*[207] gave a full depiction of the physical and chemical stability of PLA as thin films in a large range of RH environments and in contact with liquid water. Findings unambiguously showed that the PLA stability was influenced by the chemical potential and by the physical state of water molecules. This research clearly showed that the stability of PLA was influenced not only by the chemical potential of water molecules, but also by their physical state due to a different behavior of degradation products. Thus, this indicated that hydrolysis induced crystallization of MAP polymer chains, which in turn constrained additional MAP chains, transforming them into RAF.

Ming-Hung Tsai *et al.*[208] investigated effects of ultraviolet irradiation on the aging of the blends of poly(lactic acid) and poly(methyl methacrylate).They used differential scanning calorimetry to analyze the effect of ultraviolet (UV) irradiation on the physical aging of the blends of poly(lactic acid) (PLA) and poly(methyl methacrylate) (PMMA). The analyses shown the linear decrease of the maximum enthalpy loss of the aged specimen at the equilibrium state with the increase of the aging temperature, and the decreasing rate increases slightly with increasing the UV irradiation dose for the same PLA/PMMA blends. The activation energy associated with the kinetic contribution decreases with the UV irradiation dose for the PLA/PMMA blends of the same compositions.

7. Conclusion

The addition of graphene changes the properties of PLA, which will be described as follows:

✓ When using GO, brittle fracture has been observed in tensile test samples, but soft fracture has been observed when using stearic acid because the presence of stearic acid makes GO better compatible with the substrate.

✓ Dsc analysis showed that in PLA-GO nanocomposites due to the presence of graphene, the mobility of polymer chains has decreased, as a result, T_m and T_g have changed compared to pure PLA. Also, stearic acid increased the compatibility of GO with the background and increased the crystallization temperature.

✓ The use of graphene has a significant effect on the morphology of spherulite and the size of spherulite decreases with increasing amount of graphene and graphene acts as a nucleating agent.

✓ By adding graphene, the Young's modulus and tensile strength increase but the elongation decreases. In high percentages of graphene, the accumulation of nanoparticles causes lumps and decreases the strength.

✓ Graphene improves the thermal stability of PLA, and the main degradation process starts above 300 °C, which is mainly attributed to trans-esterification.

✓ In pure PLA, 72% light transmission takes place, and adding GO to the matrix reduces the transparency of PLA films, as a result, the impermeability against gases is improved.

✓ By adding graphene nano oxide, the storage modulus, loss modulus and viscosity of the complex increase compared to PLA.

✓ In the XRD analysis, the pure PLA had two sharp peaks at the angles of 16.7 and 19°, but in the nanocomposites, the peaks are in the range of about 3% compared to the pure PLA, which can be due to the very small amounts of fillers.

✓ The addition of nanographenes increases the thermal conductivity of PLA. Also, with the increase in temperature, the thermal conductivity increases due to the increase in molecular vibrations.

✓ According to the presented numerical models, the density decreases with increasing temperature.

✓ Temperature has a significant effect on rheological properties. The results show that viscosity decreases with increasing temperature (Table 2).

Conflicts of interest

There is no conflict of interest.

References

1 L. -T. Lim, T. Vanyo, J. Randall, C. Kevin and A. K. Agrawal, Processing of poly(lactic acid), *Poly(Lactic Acid) Synthesis, Structures, Properties, Processing, Applications, and End of Life*, 2022, pp. 231–270.
2 S. Ganguly and P. Das, Synthesis and Production of Polylactic Acid (PLA), in *Polylactic Acid-Based Nanocellulose and Cellulose Composites*, CRC Press, 2022, pp. 29–50.
3 C. T. Prontera, F. Villani, I. Elena Palamà, M. Grazia Maglione, P. Manini, V. Maiorano and L. Tammaro, Fabrication and biocompatibility analysis of flexible organic light emitting diodes on poly(lactic acid) substrates: toward the development of greener bio-electronic devices, *Polym. Adv. Technol.*, 2022, **33**(5), 1523–1532.
4 T. Smith, J. Feng, Z. Lu, M. Gao, M. Prévôt and S. -Q. Wang, Nanoconfined Crystallization in Poly (lactic acid)(PLA) and Poly (ethylene terephthalate)(PET) Induced by Various

Forms of Premelt-Deformation, *Macromol. Rapid Commun.*, 2022, 2200293.

5 H. Liu and J. Zhang, Research progress in toughening modification of poly (lactic acid), *J. Polym. Sci., Part B: Polym. Phys.*, 2011, **49**(15), 1051–1083.

6 I. Burzic, C. Pretschuh, D. Kaineder, G. Eder, J. Smilek, J. Másilko and W. Kateryna, Impact modification of PLA using biobased biodegradable PHA biopolymers, *Eur. Polym. J.*, 2019, **114**, 32–38.

7 F. Ebrahimi and H. Ramezani Dana, Poly lactic acid (PLA) polymers: From properties to biomedical applications, *Int. J. Polym. Mater. Polym. Biomater.*, 2022, **71**(15), 1117–1130.

8 A. Korelidou, Juan Domínguez-Robles, E. R. Magill, M. Eleftheriadou, V. A. Cornelius, R. F. Donnelly, A. Margariti and E. Larrañeta, 3D-printed reservoir-type implants containing poly (lactic acid)/poly (caprolactone) porous membranes for sustained drug delivery, *Biomater. Adv.*, 2022, **139**, 213024.

9 A. M. Pinto, S. Moreira, I. C. Gonçalves, F. M. Gama, A. M. Mendes and F. D. Magalhães, Biocompatibility of poly(lactic acid) with incorporated graphene-based materials, *Colloids Surf., B*, 2013, **104**, 229–238.

10 U. Boro, A. Priyadarsini and V. S. Moholkar, Synthesis and characterization of poly (lactic acid)/clove essential oil/alkali-treated halloysite nanotubes composite films for food packaging applications, *Int. J. Biol. Macromol.*, 2022, **216**, 927–939.

11 A. M. Abed, S. A. A. Ameer, T. H. Abdtawfeeq, A. K. Ibrahim, A. A. K. Ruhaima, A. Yada and A. R. Shariati, Effect of polarity on prediction of second order derivative thermodynamic properties of refrigerants, *Fluid Phase Equilib.*, 2023, **565**, 113652.

12 A. Abderrahmane, A. Mourad, S. Mohammed, G. F. Smaisim, D. Toghraie, A. Koulali and O. Younis, Second law analysis of a 3D magnetic buoyancy-driven flow of hybrid nanofluid inside a wavy cubical cavity partially filled with porous layer and non-Newtonian layer, *Ann. Nucl. Energy*, 2023, **181**, 109511.

13 O. Younis, A. Mourad, A. Aissa, N. A. Qasem, A. M. Abed, O. A. Akbari and A. A. Alizadeh, Numerical investigation of thermal energy storage system loaded with nano-enhanced phase change material with Koch snowflake fractal cross-section, *J. Energy Storage*, 2022, **56**, 106016.

14 G. F. Smaisim, A. M. Abed, H. Al-Madhhachi, S. K. Hadrawi, H. M. M. Al-Khateeb E. Kianfar, *Graphene-Based Important Carbon Structures and Nanomaterials for Energy Storage Applications as Chemical Capacitors and Supercapacitor Electrodes: a Review*, BioNanoScience, 2022, pp. 1–30.

15 Y. Wang, J. Zheng, G. F. Smaisim and D. Toghraie, Molecular dynamics simulation of phase transition procedure of water-based nanofluid flow containing CuO nanoparticles, *Alexandria Eng. J.*, 2022, **61**(12), 12453–12461.

16 M. Xiao and G. F. Smaisim, Joint chance-constrained multi-objective optimal function of multi-energy microgrid containing energy storages and carbon recycling system, *J. Energy Storage*, 2022, **55**, 105842.

17 A. Mourad, A. Aissa, A. M. Abed, G. F. Smaisim, D. Toghraie, M. A. Fazilati and A. A. Alizadeh, The numerical analysis of the melting process in a modified shell-and-tube phase change material heat storage system, *J. Energy Storage*, 2022, **55**, 105827.

18 H. Cheng, A. M. Abed, A. A. Alizadeh, A. A. Ghabra, F. M. Altalbawy, R. Sabetvand and Y. Riadi, The effect of temperature and external force on the thermal behavior of oil-based refrigerant inside an atomic nanochannel using molecular dynamics simulation, *J. Mol. Liq.*, 2022, 120893.

19 G. F. Smaisim, A. M. Abed and H. Alavi, Analysis of pollutant emission reduction in a coal power plant using renewable energy, *Int. J. Low-Carbon Technol.*, 2022, ctac130.

20 A. Abderrahmane, W. Jamshed, A. M. Abed, G. F. Smaisim, K. Guedri, O. A. Akbari and S. Baghaei, Heat and mass transfer analysis of non-Newtonian power-law nanofluid confined within annulus enclosure using Darcy-Brinkman-Forchheimer model, *Case Stud. Therm. Eng.*, 2022, 102569.

21 B. Freeland, E. McCarthy, R. Balakrishnan, S. Fahy, B. Adam, K. D. Rochfort, M. Dabros, R. Marti, S. M. Kelleher and J. Gaughran, A Review of Polylactic Acid as a Replacement Material for Single-Use Laboratory Components, *Materials*, 2022, **15**(9), 2989.

22 H. Zhang, Z. Qi, Z.-Y. Liu, J.-Q. Cui and X.-M. Qian, Facile fabrication of polylactic acid/polyethylene glycol micro-nano fabrics with aligned fibrous roughness for enhancing liquid anisotropic wetting performance *via* double-stage drafting melt blowing process, *Colloids Surf., A*, 2022, **648**, 129174.

23 O. M. Sanusi, A. Benelfellah, D. N. Bikiaris and N. A. Hocine, Effect of rigid nanoparticles and preparation techniques on the performances of poly (lactic acid) nanocomposites: A review, *Polym. Adv. Technol.*, 2021, **32**(2), 444–460.

24 S. Khammassi, M. Tarfaoui, K. Škrlová, D. Měřínská, D. Plachá and F. Erchiqui, Poly (Lactic Acid)(PLA)-Based Nanocomposites: Impact of Vermiculite, Silver, and Graphene Oxide on Thermal Stability, Isothermal Crystallization, and Local Mechanical Behavior, *J. Compos. Sci.*, 2022, **6**(4), 112.

25 A. Abdelrahman, F. Erchiqui and M. Nedil, Studying and evaluation physical characteristic of composite substrate chip and, its application, *Results Eng.*, 2022, **15**, 100533.

26 P. Pinthong, S. Phupaichitkun, S. Watmanee, R. Nganglumpoon, D. N. Tungasmita, S. Tungasmita, Y. Boonyongmaneerat, N. Promphet, N. Rodthongkum and J. Panpranot, Room Temperature Nanographene Production *via* CO_2 Electrochemical Reduction on the Electrodeposited Bi on Sn Substrate, *Nanomaterials*, 2022, **12**(19), 3389.

27 K. S. Novoselov, A. K. Geim, S. V. Morozov, D. Jiang, Y. Zhang, S. V. Dubonos, *et al.*, Electric Field Effect in Atomically Thin Carbon Films, *Science*, 2004, **306**, 666.

28 O. Ajala, C. Werther, P. Nikaeen, R. P. Singh and D. Depan, Influence of graphene nanoscrolls on the crystallization behavior and nano-mechanical properties of polylactic acid, *Polym. Adv. Technol.*, 2019, **30**(7), 1825–1835.

29 Y. Shibazaki, Y. Kono and G. Shen, Compressed glassy carbon maintaining graphite-like structure with linkage formation between graphene layers, *Sci. Rep.*, 2019, **9**(1), 1–8.

30 O. D. Salahdin, H. Sayadi, R. Solanki, R. Mireya, R. Parra, M. Al-Thamir, A. T. Jalil, S. E. Izzat, A. T. Hammid, L. A. B. Arenas and E. Kianfar, Graphene and carbon structures and nanomaterials for energy storage, *Appl. Phys. A: Mater. Sci. Process.*, 2022, **128**(8), 1–23.

31 X. Tan, R. F. Obaid, G. F. Smaisim, M. M. Esfahani, F. Alsaikhan, S. Baghaei and A. Yadav, Investigation of addition of calcium phosphate ceramic to multilayer scaffold for bone applications with improved mechanical properties: Fuzzy logic analysis, *Ceram. Int.*, 2022, DOI: **10.1016/j.ceramint.2022.10.366**.

32 S. Mir, A. M. Abed, O. A. Akbari, A. Mohammadian, D. Toghraie, A. Marzban and G. F. Smaisim, Effects of curvature existence, adding of nanoparticles and changing the circular minichannel shape on behavior of two-phase laminar mixed convection of Ag/water nanofluid, *Alexandria Eng. J.*, 2023, **66**, 707–730.

33 B. Ruhani, M. T. Andani, A. M. Abed, N. Sina, G. F. Smaisim, S. K. Hadrawi and D. Toghraie, Statistical modeling and investigation of thermal characteristics of a new nanofluid containing cerium oxide powder, *Heliyon*, 2022, **8**(11), e11373.

34 F. Li, A. M. Abed, O. Naghdi, N. Nasajpour-Esfahani, S. Hamedi, Z. I. Al Mashhadani and D. Toghraie, The numerical investigation of the finned double-pipe phase change material heat storage system equipped with internal vortex generator, *J. Energy Storage*, 2022, **55**, 105413.

35 W. Cai, R. Sabetvand, A. M. Abed, D. Toghraie, M. Hekmatifar, A. Rahbari and G. F. Smaisim, Thermal analysis of hydration process in the vicinity of the Copper matrix using molecular dynamics simulation for application in thermal engineering, *Energy Rep.*, 2022, **8**, 7468–7475.

36 A. Moarrefzadeh, M. R. Morovvati, S. N. Angili, G. F. Smaisim, A. Khandan and D. Toghraie, Fabrication and finite element simulation of 3D printed poly L-lactic acid scaffolds coated with alginate/carbon nanotubes for bone engineering applications, *Int. J. Biol. Macromol.*, 2022, **224**, 1496–1508.

37 B. Liu, I. Khalid, I. Patra, O. R. Kuzichkin, R. Sivaraman, A. T. Jalil and M. Hekmatifar, The effect of hydrophilic and hydrophobic surfaces on the thermal and atomic behavior of ammonia/copper nanofluid using molecular dynamics simulation, *J. Mol. Liq.*, 2022, **364**, 119925.

38 T. Hai, A. Abidi, L. Wang, A. M. Abed, M. Z. Mahmoud, E. M. T. El Din and G. F. Smaisim, Simulation of solar thermal panel systems with nanofluid flow and PCM for energy consumption management of buildings, *J. Build. Eng.*, 2022, **58**, 104981.

39 G. Fadhil Smaisim, A. M. Abed, S. K. Hadrawi and A. Shamel, Parametric investigation of thermal behaviour of salt-gradient solar pool for climatic conditions, *Clean Energy*, 2022, **6**(5), 693–704.

40 G. F. Smaisim, M. Gholami, D. Toghraie, M. Hashemian and A. M. Abed, Numerical investigation of the flow and heat transfer of Al_2O_3/water nanofluid in a tube equipped with stationary and self-rotating twisted tapes, *Prog. Nucl. Energy*, 2022, **151**, 104335.

41 M. Sang, J. Shin, K. Kim and Ki J. Yu, Electronic and thermal properties of graphene and recent advances in graphene based electronics applications, *Nanomaterials*, 2019, **9**(3), 374.

42 T. E. Twardowski, *Introduction to nanocomposite materials: properties, processing, characterization*, DEStech Publications, Inc, 2007.

43 M. R. Havstad, Biodegradable plastics, in *Plastic waste and recycling*, Academic Press, 2020, pp. 97–129.

44 L. Filiciotto and G. Rothenberg, Biodegradable plastics: Standards, policies, and impacts, *ChemSusChem*, 2021, **14**(1), 56–72.

45 M. M. Abe, J. R. Martins, P. B. Sanvezzo, J. V. Macedo, M. C. Branciforti, H. Peter, V. R. Botaro and M. Brienzo, Advantages and disadvantages of bioplastics production from starch and lignocellulosic components, *Polymers*, 2021, **13**(15), 2484.

46 R. Nandhini, B. Sivaprakash, R. Natarajan and D.-V. N. Vo, Lignin and polylactic acid for the production of bioplastics and valuable chemicals, *Environ. Chem. Lett.*, 2022, 1–25.

47 C. N. Dianursanti, L. Windiani and M. Gozan, Effect of compatibilizer addition in Spirulina platensis based bioplastic production, in *AIP Conference Proceedings*, AIP Publishing LLC, 2019, vol. 2092, no. 1, p. 030012.

48 Z.-J. Qian, J. Zhang, W.-R. Xu and Yu-C. Zhang, Development of active packaging films based on liquefied shrimp shell chitin and polyvinyl alcohol containing β-cyclodextrin/cinnamaldehyde inclusion, *Int. J. Biol. Macromol.*, 2022, **214**, 67–76.

49 I. M. Shamsuddin, J. Ahmad Jafar, A. S. A. Shawai, Y. Saleh, M. Lateefah and I. Aminu, Bioplastics as better alternative to petroplastics and their role in national sustainability: a review, *Adv. Biosci. Bioeng.*, 2017, **5**(4), 63.

50 A. Folino, A. Karageorgiou, P. S. Calabrò and D. Komilis, Biodegradation of wasted bioplastics in natural and industrial environments: A review, *Sustainability*, 2020, **12**(15), 6030.

51 Y. Jiang, G. F. Smaisim, M. Z. Mahmoud, Z. Li, H. Ş. Aybar and A. M. Abed, Simultaneous numerical investigation of the passive use of phase-change materials and the active use of a nanofluid inside a rectangular duct in the thermal management of lithium-ion batteries, *J. Power Sources*, 2022, **541**, 231610.

52 M. W. Tian, A. M. Abed, S. R. Yan, S. M. Sajadi, M. Z. Mahmoud, H. Ş. Aybar and G. F. Smaisim, Economic cost and numerical evaluation of cooling of

a cylindrical lithium-ion battery pack using air and phase change materials, *J. Energy Storage*, 2022, **52**, 104925.

53 K. A. M. Alharbi, G. F. Smaisim, S. M. Sajadi, M. A. Fagiy, H. Ş. Aybar and S. E. Elkhatib, Numerical study of lozenge, triangular and rectangular arrangements of lithium-ion batteries in their thermal management in a cooled-air cooling system, *J. Energy Storage*, 2022, **52**, 104786.

54 W. Wu, G. F. Smaisim, S. M. Sajadi, M. A. Fagiry, Z. Li, M. A. Shamseldin and H. Ş. Aybar, Impact of phase change material-based heatsinks on lithium-ion battery thermal management: A comprehensive review, *J. Energy Storage*, 2022, **52**, 104874.

55 M. W. Tian, G. F. Smaisim, S. R. Yan, S. M. Sajadi, M. Z. Mahmoud, H. Ş. Aybar and A. M. Abed, Economic cost and efficiency analysis of a lithium-ion battery pack with the circular and elliptical cavities filled with phase change materials, *J. Energy Storage*, 2022, **52**, 104794.

56 W. Brontowiyono, W. A. AbdulHussein, G. F. Smaisim, M. Z. Mahmoud, S. Singh, H. A. Lafta and S. Aravindhan, Annealing Temperature Effect on Structural, Magnetic Properties and Methyl Green Degradation of Fe_2O_3 Nanostructures, *Arabian J. Sci. Eng.*, 2022, 1–8.

57 Y. Tian, I. Patra, H. S. Majdi, N. Ahmad, R. Sivaraman, G. F. Smaisim and M. Hekmatifar, Investigation of atomic behavior and pool boiling heat transfer of water/Fe nanofluid under different external heat fluxes and forces: A molecular dynamics approach, *Case Stud. Therm. Eng.*, 2022, **38**, 102308.

58 G. F. Smaisim, H. Al-Madhhachi and A. M. Abed, Study the thermal management of Li-ion batteries using looped heat pipes with different nanofluids, *Case Stud. Therm. Eng.*, 2022, **37**, 102227.

59 G. F. Smaisim, A. M. Abed and A. Shamel, *2022, Modeling the Thermal Performance for Different Types of Solar Chimney Power Plants*, Complexity, 2022.

60 G. F. Smaisim, M. O. Bidgoli, K. L. Goh and H. Bakhtiari, Review of thermoelastic, thermal properties and creep analysis of functionally graded cylindrical shell, *Aust. J. Mech. Eng.*, 2022, 1–12.

61 A. A. Gabriel, A. F. Solikhah and A. Y. Rahmawati, Tensile strength and elongation testing for starch-based bioplastics using melt intercalation method: a review, in *Journal of Physics: Conference Series*, IOP Publishing, 2021, vol. 1858, no. 1, p. 012028.

62 W. Chartarrayawadee, R. Molloy, A. Ratchawet, N. Janmee, M. Butsamran and K. Panpai, Fabrication of poly(lactic acid)/graphene oxide/stearic acid composites with improved tensile strength, *Polym. Compos.*, 2017, **38**, 2272–2282.

63 M. Mikus and S. Galus, Biopolymers from Agriculture Waste and By-Products, in *Biopolymers*, Springer, Cham, 2022, pp. 111–128.

64 A. Pellis, M. Malinconico, A. Guarneri and L. Gardossi, Renewable polymers and plastics: Performance beyond the green, *New Biotechnol.*, 2021, **60**, 146–158.

65 A. George, M. R. Sanjay, R. Srisuk, J. Parameswaranpillai and S. Siengchin, A comprehensive review on chemical properties and applications of biopolymers and their composites, *Int. J. Biol. Macromol.*, 2020, **154**, 329–338.

66 M. Olivier and L. Avérous, Poly(lactic acid): plasticization and properties of biodegradable multiphase systems, *Polymer*, 2001, **42**(14), 6209–6219.

67 E. Balla, V. Daniilidis, G. Karlioti, T. Kalamas, M. Stefanidou, N. D. Bikiaris, A. Vlachopoulos, I. Koumentakou and D. N. Bikiaris, Poly (lactic Acid): a versatile biobased polymer for the future with multifunctional properties—From monomer synthesis, polymerization techniques and molecular weight increase to PLA applications, *Polymers*, 2021, **13**(11), 1822.

68 I. Vroman and L. Tighzert, Biodegradable Polymers, *Materials*, 2009, **2**(2), 307–344.

69 L. -T. Lim, T. Vanyo, J. Randall, C. Kevin and A. K. Agrawal, Processing of poly (lactic acid), *Poly (Lactic Acid) Synthesis, Structures, Properties, Processing, Applications, and End of Life*, 2022, pp. 231–270.

70 J.-W. Rhim, A. K. Mohanty, S. P. Singh and P. K. W. Ng, Effect of the processing methods on the performance of polylactide films: Thermocompression *versus* solvent casting, *J. Appl. Polym. Sci.*, 2006, **101**, 3736–3742.

71 G. F. Smaisim, A. M. Abed, S. K. Hadrawi and A. Shamel, Modeling and Thermodynamic Analysis of Solar Collector Cogeneration for Residential Building Energy Supply, *J. Eng.*, 2022, **2022**, 6280334.

72 M. Mozafarifard, A. Azimi, H. Sobhani, G. F. Smaisim, D. Toghraie and M. Rahmani, Numerical study of anomalous heat conduction in absorber plate of a solar collector using time-fractional single-phase-lag model, *Case Stud. Therm. Eng.*, 2022, **34**, 102071.

73 Z. M. Sharba, G. F. Smaisim, and A. A. A. Arani, Thermal Performance of Inline and Staggered Bank of Tubes with Laminar Cross Flow, in *2022 5th International Conference on Engineering Technology and its Applications (IICETA)*, 2022, May, pp. 77–84.

74 G. F. Smaisim, N. M. Prabu, A. P. Senthilkumar and A. M. Abed, Synthesis of biodiesel from fish processing waste by nano magnetic catalyst and its thermodynamic analysis, *Case Stud. Therm. Eng.*, 2022, 102115.

75 W. A. AbdulHussein, A. M. Abed, D. B. Mohammed, G. F. Smaisim and S. Baghaei, Investigation of boiling process of different fluids in microchannels and nanochannels in the presence of external electric field and external magnetic field using molecular dynamics simulation, *Case Stud. Therm. Eng.*, 2022, 102105.

76 S. Ahamad, M. Mohseni, V. Shekher, G. F. Smaisim, A. Tripathi and J. Alanya-Beltran, A Detailed Analysis of the Critical Role of artificial intelligence in Enabling High-Performance Cloud Computing Systems, in *2022 2nd International Conference on Advance Computing and Innovative Technologies in Engineering (ICACITE)*, IEEE, 2022, April, pp. 156–159.

77 A. N. Doss, D. Shah, G. F. Smaisim, M. Olha, and S. Jaiswal, A Comprehensive Analysis of Internet of Things (IOT) in

Enhancing Data Security for Better System Integrity-A Critical Analysis on the Security Attacks and Relevant Countermeasures. in *2022 2nd International Conference on Advance Computing and Innovative Technologies in Engineering (ICACITE)*, IEEE, 2022, April, pp. 165–167.

78 A. Lefteh, M. Houshmand, M. Khorrampanah, and G. F. Smaisim, Optimization of Modified Adaptive Neuro-Fuzzy Inference System (MANFIS) with Artificial Bee Colony (ABC) Algorithm for Classification of Bone Cancer, in *2022 Second International Conference on Distributed Computing and High Performance Computing (DCHPC)*, IEEE, 2022, March, pp. 78–81.

79 A. S. Sallal, G. F. Smaisim, and S. M. Thahab, The Heat Transfer from Fined Perforated Pipe Improved due to Nano-Fluid, in *Journal of Physics: Conference Series*, IOP Publishing, 2021, August, vol. 1973, No. 1, p. 012075.

80 H. Al-Madhhachi and G. F. Smaisim, Experimental and numerical investigations with environmental impacts of affordable square pyramid solar still, *Sol. Energy*, 2021, **216**, 303–314.

81 G. F. Smaisim, Investigation on heat transfer augmentation using continuous and broken ribs on a plate of heat exchanger, *Int. J. Energy Environ.*, 2018, **9**(3), 211–232.

82 H.-D. Huang, P.-G. Ren, J.-Z. Xu, L. Xu, G.-J. Zhong, B. S. Hsiao, *et al.*, Improved barrier properties of poly(lactic acid) with randomly dispersed graphene oxide nanosheets, *J. Membr. Sci.*, 2014, **464**, 110–118.

83 P. Arriagada, H. Palza, P. Palma, M. Flores and P. Caviedes, Poly (lactic acid) composites based on graphene oxide particles with antibacterial behavior enhanced by electrical stimulus and biocompatibility, *J. Biomed. Mater. Res., Part A*, 2018, **106**(4), 1051–1060.

84 T. Batakliev, V. Georgiev, C. Kalupgian, A. R. M. Pablo, H. Ribeiro, J. M. F. Guilhermino, R. J. E. Andrade, E. Ivanov and R. Kotsilkova, Physico-chemical characterization of PLA-based composites holding carbon nanofillers, *Appl. Compos. Mater.*, 2021, **28**(4), 1175–1192.

85 Y. Kang, C. Wang, Y. Qiao, J. Gu, H. Zhang, T. Peijs, J. Kong, G. Zhang and X. Shi, Tissue-engineered trachea consisting of electrospun patterned sc-PLA/GO-g-IL fibrous membranes with antibacterial property and 3D-printed skeletons with elasticity, *Biomacromolecules*, 2019, **20**(4), 1765–1776.

86 A. M. Pinto, J. Cabral, D. A. P. Tanaka, A. M. Mendes and F. D. Magalhães, Effect of incorporation of graphene oxide and graphene nanoplatelets on mechanical and gas permeability properties of poly(lactic acid) films, *Polym. Int.*, 2013, **62**, 33–40.

87 Y. Chen, X. Yao, X. Zhou, Z. Pan and Q. Gu, Poly(lactic acid)/Graphene Nanocomposites Prepared *via* Solution Blending Using Chloroform as a Mutual Solvent, *J. Nanosci. Nanotechnol.*, 2011, **11**, 7813–7819.

88 Y. Chen, X. Yao, Q. Gu and Z. Pan, Non-isothermal crystallization kinetics of poly (lactic acid)/graphene nanocomposites, *J. Polym. Eng.*, 2013, 163.

89 M. Sabzi, L. Jiang, F. Liu, I. Ghasemi and M. Atai, Graphene nanoplatelets as poly (lactic acid) modifier: linear rheological behavior and electrical conductivity, *J. Mater. Chem. A*, 2013, **1**(28), 8253–8261.

90 B. W. Chieng, N. A. Ibrahim, W. Md Z. W. Yunus, M. Z. Hussein and V. S. Giita Silverajah, Graphene nanoplatelets as novel reinforcement filler in poly (lactic acid)/epoxidized palm oil green nanocomposites: Mechanical properties, *Int. J. Mol. Sci.*, 2012, **13**(9), 10920–10934.

91 W. Yu, S. Li, H. Yang and J. Luo, Progress in the functional modification of graphene/graphene oxide: A review, *RSC Adv.*, 2020, **10**(26), 15328–15345.

92 B. Azizi, M. Shariati, S. S. M. N. Souq and M. Hosseini, Bending and stretching behavior of graphene structures using continuum models calibrated with modal analysis, *Appl. Math. Model.*, 2023, **114**, 466–487.

93 B. Azizi, M. Hosseini, and M. Shariati, On the hybrid atomistic-continuum model for vibrational analysis of α-, β-, and γ-graphyne circular nano-plates, *Waves in Random and Complex Media*, 2022, pp. 1–36.

94 M. Shariati, S. S. M. N. Souq and B. Azizi, Surface-and nonlocality-dependent vibrational behavior of graphene using atomistic-modal analysis, *Int. J. Mech. Sci.*, 2022, **228**, 107471.

95 M. Duffer, *Two Stream Instability in Graphene*, 2018.

96 C. Gao, P. Liu, Y. Ding, T. Li, F. Wang, J. Chen, S. Zhang, Z. Li and M. Yang, Non-contact percolation of unstable graphene networks in poly (styrene-co-acrylonitrile) nanocomposites: Electrical and rheological properties, *Compos. Sci. Technol.*, 2018, **155**, 41–49.

97 R. Momen, R. Rezaee, B. Azizi, S. Rezaee, H. Hou and X. Ji, Evaluation of mechanical properties of multilayer graphyne-based structures as anode materials for lithium-ions batteries, *Eur. Phys. J. Plus*, 2022, **137**(3), 360.

98 G. F. Smaisim, A. M. Abed, H. Al-Madhhachi, S. K. Hadrawi, H. M. M. Al-Khateeb and E. Kianfar, Graphene-Based Important Carbon Structures and Nanomaterials for Energy Storage Applications as Chemical Capacitors and Supercapacitor Electrodes: a Review, *BioNanoScience*, 2022, 1–30.

99 O. D. Salahdin, H. Sayadi, R. Solanki, R. Mireya, R. Parra, M. Al-Thamir, A. T. Jalil, S. E. Izzat, A. T. Hammid, L. A. B. Arenas and E. Kianfar, Graphene and carbon structures and nanomaterials for energy storage, *Appl. Phys. A: Mater. Sci. Process.*, 2022, **128**(8), 1–23.

100 K. S. Novoselov, A. K. Geim, S. V. Morozov, D. Jiang, M. I. Katsnelson, I. V. Grigorieva, *et al.*, Two-dimensional gas of massless Dirac fermions in graphene, *Nature*, 2005, **438**, 197200.

101 W. K. Abdelbasset, S. A. Jasim, D. O. Bokov, M. S. Oleneva, A. Islamov, A. T. Hammid, Y. F. Mustafa, G. Yasin, A. C. Alguno and E. Kianfar, Comparison and evaluation of the performance of graphene-based biosensors, *Carbon Lett.*, 2022, 1–25.

102 X. Zhang, Y. Tang, F. Zhang and C. -S. Lee, A novel aluminum-graphite dual-ion battery, *Adv. Energy Mater.*, 2016, **6**(11), 1502588.

103 S. Reich, J. Maultzsch, C. Thomsen and P. Ordejón, Tight-binding description of graphene, *Phys. Rev. B*, 2002, **66**, 035412.

104 Y. W. Sun, D. G. Papageorgiou, C. J. Humphreys, D. J. Dunstan, P. Puech, J. E. Proctor, C. Bousige, D. Machon and A. San-Miguel, Mechanical properties of graphene, *Appl. Phys. Rev.*, 2021, **8**(2), 021310.

105 M. Koshino, Electronic transport in bilayer graphene, *New J. Phys.*, 2009, **11**, 095010.

106 H. Horii, M. Matsubara, K. Sasaoka, T. Yamamoto and H. Fukuyama, Optimization of Thermoelectric Power Factor of Bilayer Graphene by Vertical Electric Field, *J. Phys. Soc. Jpn.*, 2021, **90**(10), 104711.

107 H. Horii, M. Matsubara, K. Sasaoka and T. Yamamoto, Maximum Thermoelectric Power Factor and Optimal Carrier Concentration of Bilayer Graphene at Various Temperatures, *e-J. Surf. Sci. Nanotechnol.*, 2021, **19**, 125–130.

108 X. L. Liu, J. Liu, H. Ma Yang, Bo Huang and G. H. Zeng, Design of a high-performance graphene/SiO 2-Ag periodic grating/MoS 2 surface plasmon resonance sensor, *Appl. Opt.*, 2022, **61**(23), 6752–6760.

109 M. Shi, R. Wang, L. Li, N. Chen, P. Xiao, C. Yan and X. Yan, Redox-Active Polymer Integrated with MXene for Ultra-Stable and Fast Aqueous Proton Storage, *Adv. Funct. Mater.*, 2022, 2209777.

110 M. Shi, H. Zhu, C. Chen, J. Jiang, L. Zhao and C. Yan, Synergistically coupling of graphene quantum dots with Zn-intercalated MnO_2 cathode for high-performance aqueous Zn–ion batteries, *Int. J. Miner., Metall. Mater.*, 2023, **30**(1), 25–32.

111 I. Chakraborty, K. J. Bodurtha, N. J. Heeder, M. P. Godfrin, A. Tripathi, R. H. Hurt, A. Shukla and A. Bose., Massive electrical conductivity enhancement of multilayer graphene/polystyrene composites using a nonconductive filler, *ACS Appl. Mater. Interfaces*, 2014, **6**(19), 16472–16475.

112 Q. Zhang, X. Cheng, C. Wang, A. M. Rao and B. Lu, Sulfur-assisted large-scale synthesis of graphene microspheres for superior potassium-ion batteries, *Energy Environ. Sci.*, 2021, **14**(2), 965–974.

113 C. Bie, H. Yu, B. Cheng, W. Ho, J. Fan and J. Yu, Design, fabrication, and mechanism of nitrogen-doped graphene-based photocatalyst, *Adv. Mater.*, 2021, **33**(9), 2003521.

114 R. Harichandran, R. Vignesh Kumar and M. Venkateswaran, Experimental and numerical evaluation of thermal conductivity of graphene nanoplatelets reinforced aluminium composites produced by powder metallurgy and hot extrusion technique, *J. Alloys Compd.*, 2022, **900**, 163401.

115 Y. Chen, J. Long, B. Xie, Y. Kuang, X. Chen, M. Hou, J. Gao, H. Liu, Y. He and C.-P. Wong, One-Step Ultraviolet Laser-Induced Fluorine-Doped Graphene Achieving Superhydrophobic Properties and Its Application in Deicing, *ACS Appl. Mater. Interfaces*, 2022, **14**(3), 4647–4655.

116 Le Li, D. Zhang, J. Deng, Y. Gou, J. Fang, H. Cui, Y. Zhao and M. Cao, Carbon-based materials for fast charging lithium-ion batteries, *Carbon*, 2021, **183**, 721–734.

117 B. Azizi, S. Rezaee, M. J. Hadianfard and K. H. Dehnou, A comprehensive study on the mechanical properties and failure mechanisms of graphyne nanotubes (GNTs) in different phases, *Comput. Mater. Sci.*, 2020, **182**, 109794.

118 S. Ziraki, S. M. Zebarjad and M. J. Hadianfard, A study on the role of polypropylene fibers and silica nanoparticles on the compression properties of silicone rubber composites as a material of finger joint implant, *Int. J. Polym. Mater. Polym. Biomater.*, 2017, **66**(1), 48–52.

119 M. Pavía, K. Alajami, P. Estellé, D. Alexandre and B. Vigolo, A critical review on thermal conductivity enhancement of graphene-based nanofluids, *Adv. Colloid Interface Sci.*, 2021, **294**, 102452.

120 H. Peng, X. Ming, K. Pang, Y. Chen, J. Zhou, Z. Xu, Y. Liu and C. Gao, Highly electrically conductive graphene papers *via* catalytic graphitization, *Nano Res.*, 2022, 1–7.

121 H. Murata, Y. Nakajima, N. Saitoh, N. Yoshizawa, T. Suemasu and K. Toko, High-electrical-conductivity multilayer graphene formed by layer exchange with controlled thickness and interlayer, *Sci. Rep.*, 2019, **9**(1), 1–5.

122 G. F. Smaisim, Augmentation of Heat Transfer in Corrugated Tube Using Four-Start Spiral Wall, *Al-Qadisiyah J. Eng. Sci.*, 2017, **10**(4), 451–467.

123 G. F. Smaisim, Enhancement Heat Transfer of Cu-Water Nanofluids with Thermophysical Properties Modeling by Artificial Neural Network, *J. Univ. Babylon*, 2017, **25**(5), 1721–1735.

124 G. Smaisim, O. Fatta, A. Valera-Medina, A. Rageb, and N. Syred, Investigation of heat transfer and fluid mechanics across a heated rotating circular cylinder in crossflow, in *54th AIAA Aerospace Sciences Meeting*, 2016, p. 0494.

125 G. Smaisim, O. Fatla, A. Valera Medina, A. M. Rageb and N. Syred, Experimental and theoretical investigation of the effect of rotating circular cylinder speed on the lift and drag forces, *Int. J. Energy Environ.*, 2016, **7**(1), 23–36.

126 M. Yang, C. Li, Y. Zhang, D. Jia, X. Zhang, Y. Hou, R. Li and J. Wang, Maximum undeformed equivalent chip thickness for ductile-brittle transition of zirconia ceramics under different lubrication conditions, *Int. J. Mach. Tools Manuf.*, 2017, **122**, 55–65, DOI: **10.1016/j.ijmachtools.2017.06.003**.

127 M. Yang, C. Li, Y. Zhang, D. Jia, R. Li, Y. Hou, H. Cao and J. Wang, Predictive model for minimum chip thickness and size effect in single diamond grain grinding of zirconia ceramics under different lubricating conditions, *Ceram. Int.*, 2019, **45**(12), 14908–14920, DOI: **10.1016/j.ceramint.2019.04.226**.

128 J. Zhang, C. Li, Y. Zhang, M. Yang, D. Jia, G. Liu, Y. Hou, R. Li, N. Zhang, Q. Wu and H. Cao, Experimental assessment of an environmentally friendly grinding process using nanofluid minimum quantity lubrication

with cryogenic air, *J. Cleaner Prod.*, 2018, **193**, 236–248, DOI: 10.1016/j.jclepro.2018.05.009.

129 D. Jia., Y. Zhang., Li. Changhe, Y. Min, T. Gao., Z. Said. and S. Sharma., Lubrication-enhanced mechanisms of titanium alloy grinding using lecithin biolubricant, *Tribol. Int.*, 2022, **169**, 107461, DOI: 10.1016/j.triboint.2022.107461.

130 W. Xu, C. Li, Y. Zhang, H. M. Ali, S. Sharma, R. Li, M. Yang, T. Gao, M. Liu, X. Wang, Z. Said, X. Liu and Z. Zou, Electrostatic atomization minimum quantity lubrication machining: from mechanism to application, *Int. J. Extrem. Manuf.*, 2022, **4**, 042003, DOI: 10.1088/2631-7990/ac9652.

131 M. Liu, C. Li, Y. Zhang, M. Yang, T. Gao, X. Cui, X. Wang, W. Xu, Z. Zhou, B. Liu, Z. Said, R. Li and S. Sharma, Analysis of grinding mechanics and improved grinding force model based on randomized grain geometric characteristics, *Chin. J. Aeronaut.*, 2022, DOI: 10.1016/j.cja.2022.11.005.

132 P. Wilhelm, T. C. Lang and A. M. Läuchli, Interplay of fractional Chern insulator and charge density wave phases in twisted bilayer graphene, *Phys. Rev. B*, 2021, **103**(12), 125406.

133 R. I. Harrysson, A. Generalov, M. Soikkeli, A. Murros, S. Arpiainen, and A. Vorobiev, Geometrical magnetoresistance effect and mobility in graphene field-effect transistors, *arXiv*, 2022, preprint, arXiv: 2205.15177.

134 A. Mousa, *Optical response of graphene under strain*, 2022.

135 G. Lopez-Polin, C. Gomez-Navarro and J. Gomez-Herrero, The effect of rippling on the mechanical properties of graphene, *Nano Mater. Sci.*, 2022, **4**(1), 18–26.

136 Y. Gong, L. Shen, Z. Kang, K. Liu, Q. Du, D. Ye, H. Zhao, X. A. Sun and J. Zhang, Progress in energy-related graphyne-based materials: advanced synthesis, functional mechanisms and applications, *J. Mater. Chem. A*, 2020, **8**(41), 21408–21433.

137 N. Baig, I. Kammakakam and W. Falath, Nanomaterials: A review of synthesis methods, properties, recent progress, and challenges, *Mater. Adv.*, 2021, **2**(6), 1821–1871.

138 A. K. Geim and K. S. Novoselov, The rise of graphene, *Nat. Mater.*, 2007, **6**, 183.

139 S.-W. Kim, H.-K. Kim, K. Lee, K. C. Roh, J. T. Han, K.-B. Kim, S. Lee and M.-H. Jung, Studying the reduction of graphene oxide with magnetic measurements, *Carbon*, 2019, **142**, 373–378.

140 S. Park and R. S. Ruoff, Chemical methods for the production of graphenes, *Nat. Nanotechnol.*, 2009, **4**, 217.

141 Y. M. Manawi, A. Samara, T. Al-Ansari and M. A. Atieh, A review of carbon nanomaterials' synthesis *via* the chemical vapor deposition (CVD) method, *Materials*, 2018, **11**(5), 822.

142 L. Sun, G. Yuan, L. Gao, J. Yang, M. Chhowalla, Meysam Heydari Gharahcheshmeh, K. K. Gleason, Y. S. Choi, B. H. Hong and Z. Liu., Chemical vapour deposition, *Nat. Rev. Methods Primers*, 2021, **1**(1), 1–20.

143 X. Li, W. Cai, J. An, S. Kim, J. Nah, D. Yang, *et al.*, Large-Area Synthesis of High-Quality and Uniform Graphene Films on Copper Foils, *Science*, 2009, **324**, 1312.

144 P. P. Brisebois and S. Mohamed, Harvesting graphene oxide–years 1859 to 2019: a review of its structure, synthesis, properties and exfoliation, *J. Mater. Chem. C*, 2020, **8**(5), 1517–1547.

145 M. Yi and Z. Shen, A review on mechanical exfoliation for the scalable production of graphene, *J. Mater. Chem. A*, 2015, **3**, 11700–11715.

146 F. Pogacean, M. Coros, V. Mirel, L. Magerusan, L. Barbu-Tudoran, A. Vulpoi, R.-I. S.-van Staden and S. Pruneanu, Graphene-based materials produced by graphite electrochemical exfoliation in acidic solutions: Application to Sunset Yellow voltammetric detection, *Microchem. J.*, 2019, **147**, 112–120.

147 F. Liu, C. Wang, S. Xiao, M. Adil Riaz, M. Xu, W. Li and Y. Chen, Synthesis of graphene materials by electrochemical exfoliation: Recent progress and future potential, *Carbon Energy*, 2019, **1**(2), 173–199.

148 M. J. Allen, V. C. Tung and R. B. Kaner, Honeycomb Carbon: A Review of Graphene, *Chem. Rev.*, 2010, **110**, 132–145.

149 W. S. Hummers and R. E. Offeman, Preparation of Graphitic Oxide, *J. Am. Chem. Soc.*, 1958, **80**, 1339.

150 M. N. Nair, A. Celis, F. Nicolas, S. Kubsky, A. Taleb-Ibrahimi and A. Tejeda., Substrate effect on the electronic properties of graphene on vicinal Pt (1 1 1), *Appl. Surf. Sci.*, 2021, **565**, 150593.

151 M. Sang, J. Shin, K. Kim and Ki J. Yu, Electronic and thermal properties of graphene and recent advances in graphene based electronics applications, *Nanomaterials*, 2019, **9**(3), 374.

152 A. Osman, A. Elhakeem, S. Kaytbay and A. Ahmed, Thermal, electrical and mechanical properties of graphene/nano-alumina/epoxy composites, *Mater. Chem. Phys.*, 2021, **257**, 123809.

153 Y.-seok Jun, S. Habibpour, M. Hamidinejad, M. Gyu Park, W. Ahn, A. Yu and Chul B. Park, Enhanced electrical and mechanical properties of graphene nano-ribbon/thermoplastic polyurethane composites, *Carbon*, 2021, **174**, 305–316.

154 M. Hamrahjoo, S. Hadad, E. Dehghani, M. Salami-Kalajahi and H. Roghani-Mamaqani, Poly (poly [ethylene glycol] methyl ether methacrylate)/graphene oxide nanocomposite gel polymer electrolytes prepared by controlled and conventional radical polymerizations for lithium ion batteries, *Int. J. Energy Res.*, 2022, **46**(7), 9114–9127.

155 Y. Fadil, S. C. Thickett, V. Agarwal and P. B. Zetterlund., Synthesis of graphene-based polymeric nanocomposites using emulsion techniques, *Prog. Polym. Sci.*, 2022, **125**, 101476.

156 H. Lin, Q. Jian, X. Bai, D. Li, Z. Huang, W. Huang, S. Feng and Z. Cheng, Recent advances in thermal conductivity and thermal applications of graphene and its derivatives nanofluids, *Appl. Therm. Eng.*, 2022, 119176.

157 R. B. Valapa, G. Pugazhenthi and V. Katiyar, Effect of graphene content on the properties of poly(lactic acid) nanocomposites, *RSC Adv.*, 2015, **5**, 28410–28423.

158 I. S. Bayer, Thermomechanical properties of polylactic acid-graphene composites: A state-of-the-art review for biomedical applications, *Materials*, 2017, **10**(7), 748.

159 I. Kiran, N. Akhtar Shad, M. Munir Sajid, Y. Jamil, Y. Javed, M. Irfan Hussain, and K. Akhtar, Graphene Functionalized PLA Nanocomposites and Their Biomedical Applications, in *Graphene Based Biopolymer Nanocomposites*, Springer, Singapore, 2021, pp. 83–105.

160 T. W. Clyne, and D. Hull, *An introduction to composite materials*, Cambridge university press, 2019.

161 S. W. Tsai, and H. Thomas Hahn, *Introduction to composite materials*, Routledge, 2018.

162 E. Omanović-Mikličanin, A. Badnjević, A. Kazlagić and M. Hajlovac., Nanocomposites: A brief review, *Health Technol.*, 2020, **10**(1), 51–59.

163 A. D. de Oliveira and C. A. G. Beatrice, Polymer nanocomposites with different types of nanofiller, *Nanocomposites-Recent Evolutions*, 2018, 103–104.

164 L. S. De Bortoli, R. de Farias, D. Z. Mezalira, L. M. Schabbach and M. C. Fredel, Functionalized carbon nanotubes for 3D-printed PLA-nanocomposites: Effects on thermal and mechanical properties, *Mater. Today Commun.*, 2022, **31**, 103402.

165 S. Rogovina, S. Lomakin, S. Usachev, M. Gasymov, O. Kuznetsova, N. Shilkina, V. Shevchenko, A. Shapagin, E. Prut and A. Berlin, The Study of Properties and Structure of Polylactide–Graphite Nanoplates Compositions, *Polym. Cryst*, 2022, **2022**, 4367582.

166 J. M. Prabhudass, K. Palanikumar, E. Natarajan and K. Markandan, Enhanced Thermal Stability, Mechanical Properties and Structural Integrity of MWCNT Filled Bamboo/Kenaf Hybrid Polymer Nanocomposites, *Materials*, 2022, **15**(2), 506.

167 I. Montes-Zavala, M. J. Pérez-González, E. O. Castrejón-González, D. A. Santamaría-Razo, A. Almendárez-Camarillo, E. Pérez and J. A. Gonzalez-Calderon, Thermal and mechanical properties of poly (lactic acid) filled with modified silicon dioxide: importance of the surface area, *Polym. Bull.*, 2022, **79**(3), 1409–1435.

168 A. Mishra, M. Shukla, M. K. Shukla, D. Srivastava and A. K. Nagpal, Thermal and mechanical characterization of alumina modified multifunctional novolac epoxy nanocomposites, *Polym. Polym. Compos.*, 2022, **30**, 09673911221081827.

169 A. Gacem, M. S. Refat, H. E. Ali, S. C. V. Naidu, B. Beenarani, P. Deole, S. Sandeep Kumar, S. Rama, A. M. Alsuhaibani and D. Abdi, Optimization and Mechanical Characteristics of AA6061/Zirconia Nanocomposites Fabricated by Ultrasonic-Aided Stir Casting Method, *J. Nanomater.*, 2022, 2453412.

170 H.-fei Zhong, W.-hua Xu, H. Xie, T. Wu and J.-ping Qu, Cost-Effective Fabrication of High-Density Polyethylene/Graphene Nanocomposites by an *In Situ* Exfoliation Method Based on a Series Explosion Effect, *Ind. Eng. Chem. Res.*, 2022, **61**(31), 11474–11483.

171 F. Arianpour, J. Mansour, S. Abedi, F. Vafaee, A. Qahtan, Yousif and M. Salavati-Niasari, *In situ* polymerization of silica/polyethylene using bisupported Ziegler-Natta catalyst of nanosilica/BOM/$TiCl_4$/TEAL: Study of thermo-mechanical properties system, *Inorg. Chem. Commun.*, 2022, **143**, 109726.

172 A. Kamal, M. Ashmawy, A. M. Algazzar and A. H. Elsheikh, Fabrication techniques of polymeric nanocomposites: A comprehensive review, *Proc. Inst. Mech. Eng., Part C*, 2022, **236**(9), 4843–4861.

173 M. S. A. Darwish, M. H. Mostafa and L. M. Al-Harbi, Polymeric Nanocomposites for Environmental and Industrial Applications, *Int. J. Mol. Sci.*, 2022, **23**(3), 1023.

174 M. S. A. Darwish, M. H. Mostafa and L. M. Al-Harbi, Polymeric Nanocomposites for Environmental and Industrial Applications, *Int. J. Mol. Sci.*, 2022, **23**(3), 1023.

175 R. Megherbi, L. Mrah and M. Marref, Maghnite: an innovative inorganic reinforcement used in the synthesis of polystyrene nanocomposites with optimized thermal and mechanical properties, *Iran. Polym. J.*, 2022, **31**(2), 223–236.

176 N. Zhang, Largely Improved Mechanical Properties of Polyurethane Nanocomposites *via In Situ* Polymerization with Low Loading of Graphene Oxide, *J. Macromol. Sci., Part B: Phys.*, 2022, 1–13.

177 Y. Fadil, S. C. Thickett, V. Agarwal and P. B. Zetterlund, Synthesis of graphene-based polymeric nanocomposites using emulsion techniques, *Prog. Polym. Sci.*, 2022, **125**, 101476.

178 Y. S. Khoo, W. J. Lau, Y. Y. Liang, M. Karaman, M. Gürsoy and A. F. Ismail, Eco-friendly surface modification approach to develop thin film nanocomposite membrane with improved desalination and antifouling properties, *J. Adv. Res.*, 2022, **36**, 39–49.

179 V. D. Thuc, V. D. C. Tinh and D. Kim, Simultaneous improvement of proton conductivity and chemical stability of Nafion membranes *via* embedment of surface-modified ceria nanoparticles in membrane surface, *J. Membr. Sci.*, 2022, **642**, 119990.

180 V. Tirth, S. W. Ghori, and P. Gupta, Fundamentals of polymer nanocomposites, in *Advanced Polymer Nanocomposites*, Woodhead Publishing, 2022, pp. 3–27.

181 H. C. Kim, P. S. Panicker, R. M. Muthoka, J. Jang, Yi Sung, and J. Kim, A study in bio-nanocomposite based on polycaprolactone reinforced by cellulose nanocrystal, in *Nano-, Bio-, Info-Tech Sensors, and Wearable Systems*, SPIE, 2022, vol. 12045, pp. 104–108.

182 H. Kim and C. W. Macosko, Processing-property relationships of polycarbonate/graphene composites, *Polymer*, 2009, **50**, 3797–3809.

183 H. Kim and C. W. Macosko, Morphology and Properties of Polyester/Exfoliated Graphite Nanocomposites, *Macromolecules*, 2008, **41**, 3317–3327.

184 J. Liang, Y. Wang, Y. Huang, Y. Ma, Z. Liu, J. Cai, *et al.*, Electromagnetic interference shielding of graphene/epoxy composites, *Carbon*, 2009, **47**, 922–925.

185 J. Y. Jang, M. S. Kim, H. M. Jeong and C. M. Shin, Graphite oxide/poly(methyl methacrylate) nanocomposites prepared

by a novel method utilizing macroazoinitiator, *Compos. Sci. Technol.*, 2009, **69**, 186–91.

186 S. Park, J. An, I. Jung, R. D. Piner, S. J. An, X. Li, *et al.*, Colloidal Suspensions of Highly Reduced Graphene Oxide in a Wide Variety of Organic Solvents, *Nano Lett.*, 2009, **9**, 1593–1597.

187 S. Villar-Rodil, J. I. Paredes, A. Martínez-Alonso and J. M. D. Tascón, Preparation of graphene dispersions and graphene-polymer composites in organic media, *J. Mater. Chem.*, 2009, **19**, 3591–3593.

188 L. Zhang, Y. Li, H. Wang, Y. Qiao, J. Chen and S. Cao, Strong and ductile poly(lactic acid) nanocomposite films reinforced with alkylated graphene nanosheets, *Chem. Eng. J.*, 2015, **264**, 538–546.

189 T.-R. Kuang, H.-Y. Mi, D.-J. Fu, X. Jing, B.-Y. Chen, W.-J. Mou, *et al.*, Fabrication of Poly(lactic acid)/Graphene Oxide Foams with Highly Oriented and Elongated Cell Structure *via* Unidirectional Foaming Using Supercritical Carbon Dioxide, *Ind. Eng. Chem. Res.*, 2015, **54**, 758–768.

190 S. W. Kim and H. M. Choi, Morphology, thermal, mechanical, and barrier properties of graphene oxide/poly(lactic acid) nanocomposite films, *Korean J. Chem. Eng.*, 2016, **33**, 330–336.

191 C. H. Chan, C. H. Chia, S. Zakaria, I. Ahmad and A. Dufresne, low filler content cellulose nanocrystal and graphene oxide reinforced polylactic acid film composites, *Polym. Res. J.*, 2015, **33**, 165–177.

192 L. Zhao, X. Liu, R. Zhang, H. He, T. Jin and J. Zhang, Unique Morphology in Polylactide/Graphene Oxide Nanocomposites, *J. Macromol. Sci., Part B: Phys.*, 2015, **54**, 45–57.

193 D. Wu, H. Xu and M. Hakkarainen, From starch to polylactide and nano-graphene oxide: fully starch derived high performance composites, *RSC Adv.*, 2016, **6**(59), 54336–54345.

194 Lu He, F. Song, Li De-Fu, Xi Zhao, X.-Li Wang and Yu-Z. Wang, Strong and tough polylactic acid based composites enabled by simultaneous reinforcement and interfacial compatibilization of microfibrillated cellulose, *ACS Sustainable Chem. Eng.*, 2020, **8**(3), 1573–1582.

195 L. Chen, H. M. Wong, K. W. K. Yeung and S. Chin Tjong, Novel electrospun polylactic acid nanocomposite fiber mats with hybrid graphene oxide and nanohydroxyapatite reinforcements having enhanced biocompatibility, *Polymers*, 2016, **8**(8), 287.

196 M. K. Patel, F. Hansson, O. Pitkänen, S. Geng and K. Oksman, Biopolymer Blends of Poly (Lactic Acid) and Poly (Hydroxybutyrate) and Their Functionalization with Glycerol Triacetate and Chitin Nanocrystals for Food Packaging Applications, *ACS Appl. Polym. Mater.*, 2022, **4**(9), 6592–6601.

197 H. Xu, M. Shen, S. Han, W. Xu, S. Zhang, H.-R. Yang, D. Zhou and M. Hakkarainen, Osteoconductive and antibacterial poly (lactic acid) fibrous membranes impregnated with biobased nanocarbons for biodegradable bone regenerative scaffolds, *Ind. Eng. Chem. Res.*, 2021, **60**(32), 12021–12031.

198 A. Rostami, H. Nazockdast and M. Karimi, Graphene induced microstructural changes of PLA/MWCNT biodegradable nanocomposites: rheological, morphological, thermal and electrical properties, *RSC Adv.*, 2016, **6**(55), 49747–49759.

199 A. Nuona, X. Li, X. Zhu, Y. Xiao and J. Che, Starch/polylactide sustainable composites: Interface tailoring with graphene oxide, *Composites, Part A*, 2015, **69**, 247–254.

200 Z. Oluz and T. Tinçer, Additives for ultraviolet-induced oxidative degradation of lowdensity polyethylene, *J. Appl. Polym. Sci.*, 2016, **133**(17), 43354.

201 S. Nikafshar, O. Zabihi, M. Ahmadi, A. Mirmohseni, M. Taseidifar and M. Naebe, The Effects of UV Light on the Chemical and Mechanical Properties of a Transparent Epoxy-Diamine System in the Presence of an Organic UV Absorber, *Materials*, 2017, **10**(2), 180.

202 G. Spinelli, R. Guarini, R. Kotsilkova, T. Batakliev, E. Ivanov and V. Romano, Experimental and Simulation Studies of Temperature Effect on Thermophysical Properties of Graphene-Based Polylactic Acid, *Materials*, 2022, **15**(3), 986.

203 O. T. Adesina, E. R. Sadiku, T. Jamiru, O. F. Ogunbiyi, L. W. Beneke and A. T. Adegbola, Optimization of SPS processing parameters on the density and hardness properties of graphene reinforced polylactic acid nanocomposite, *Int. J. Adv. Manuf. Technol.*, 2019, **102**(9), 4047–4058.

204 Yu, W. Wang, J. Zhang, J. R. Wu, X. Z. Wang and Yu He Deng, Incorporation of graphitic nano-filler and poly (lactic acid) in fused deposition modeling, *J. Appl. Polym. Sci.*, 2017, **134**(15), 44703.

205 Qi. Zhang, *Fabricating and Characterizing Multifunctional Graphene Nanoplatelets-based Polylactide Nanocomposites*, 2020.

206 M. K. Lila, K. Shukla, U. Kumar Komal and I. Singh, Accelerated thermal ageing behaviour of bagasse fibers reinforced Poly (Lactic Acid) based biocomposites, *Composites, Part B*, 2019, **156**, 121–127.

207 J. R. Rocca-Smith, O. Whyte, C.-H. Brachais, D. Champion, F. Piasente, E. Marcuzzo, A. Sensidoni, F. Debeaufort and T. Karbowiak, Beyond biodegradability of poly (lactic acid): physical and chemical stability in humid environments, *ACS Sustainable Chem. Eng.*, 2017, **5**(3), 2751–2762.

208 M.-H. Tsai, H. Ouyang, F. Yang, M.-K. Wei and S. Lee, Effects of ultraviolet irradiation on the aging of the blends of poly (lactic acid) and poly (methyl methacrylate), *Polymer*, 2022, 124947.